CHAPTER

Photovoltaic Systems

9

Photovoltaic (PV) modules are solid-state devices that convert sunlight, the most abundant energy source on the planet, directly into electricity without an intervening heat engine or rotating equipment. PV equipment has no moving parts and, as a result, requires minimal maintenance and has a long life. It generates electricity without producing emissions of greenhouse or any other gases and its operation is virtually silent. Photovoltaic systems can be built in virtually any size, ranging from milliwatt to megawatt, and the systems are modular, i.e., more panels can be easily added to increase output. Photovoltaic systems are highly reliable and require little maintenance. They can also be set up as stand-alone systems.

A PV cell consists of two or more thin layers of semiconducting material, most commonly silicon. When the silicon is exposed to light, electrical charges are generated; and this can be conducted away by metal contacts as direct current. The electrical output from a single cell is small, so multiple cells are connected and encapsulated (usually glass covered) to form a module (also called a *panel*). The PV panel is the main building block of a PV system, and any number of panels can be connected together to give the desired electrical output. This modular structure is a considerable advantage of the PV system, where further panels can be added to an existing system as required.

In the early days of photovoltaics, some 50 years ago, the energy required to produce a PV panel was more than the energy the panel could produce during its lifetime. During the last decade, however, due to improvements in the efficiency of the panels and manufacturing methods, the payback times have fallen to 2–3 years for crystalline silicon PV systems, and to almost one year for some thin-film systems, under moderate levels of sunshine (Fthenakis and Kim, 2011).

Photovoltaic prices have fallen sharply since the mid-1970s. It is generally believed that, as photovoltaic prices fall, markets will expand rapidly. Worldwide photovoltaic sales are about 2500 MWe annually (2006 values) and the increase from 2005 was 40% (Sayigh, 2008). The major problem limiting the widespread use of photovoltaics is the high cost of manufacturing the sheets of semiconductor materials needed for power systems. However, the cost of PV panels has also fallen markedly—both of crystalline silicon, as manufacturing output particularly in China has increased, and of thin-film, where large-scale manufacturing has commenced. In 2012 the market prices of PV modules had fallen to less than $0.80 per Watt, compared to around $2 per Watt in 2010 and $5 per Watt in 2000. A large thin-film PV producer, First Solar, expects its manufacturing cost to be less than $0.60 per Watt by 2014.

Falling module prices coupled with government incentives—notably feed-in tariffs in Europe and investment tax credits in the US—have caused the market for photovoltaics to grow rapidly in recent years (RENI, 2010; Price and Margolis, 2010). In 2000 the installed PV capacity worldwide was

Solar Energy Engineering. http://dx.doi.org/10.1016/B978-0-12-397270-5.00009-1

1.4 GW (EPIA, 2010); at the end of 2011 it had reached 67 GW (Photon, 2012a) and another 31 GW was expected to be added in 2012 (Photon, 2012b).

Despite achieving a mass-production scale and lower manufacturing costs, utility-scale PV is still more expensive than both fossil fuels and other renewable energies (Tidball et al., 2010). This holds for both its capital cost, where large PV projects typically cost $2.50–4 per Watt (Barbose et al., 2011), and its average cost of electricity of $0.17 per kWh. Residential PV systems are slightly more expensive, at roughly $5 in the US and $4 per Watt in Germany, without incentives (Barbose et al., 2011).

The gap is narrowing however. As of 2012, large PV plants in areas with high irradiance were estimated to generate electricity for as little as $0.10 per kWh. As a result, solar power has been found to be more economical than fossil fuels in an increasing number of real-world situations, such as for peak-load power or when compared to oil-burning power plants. It is also noteworthy that PV has become around a third cheaper than concentrating solar power, in terms of cost of per kWh of electricity, as PV module prices have fallen.

PV possesses other advantages that can justify its higher price: It produces no greenhouses gases, and relative to other renewables; it can be installed in a wider variety of places (for example on rooftops and parking shades); additional modules can be added incrementally; a utility-scale power plant can be constructed in months; and PV requires very little maintenance (Price and Margolis, 2010; Tidball et al., 2010). Also PV produces electricity during the afternoon when demand is highest, and it is often sited close to electricity users, which reduces transmission costs. These factors make electricity from PV more "valuable" than that from a traditional power station.

Costs can be reduced through several alternative paths. Systems based on thin films of materials, such as amorphous silicon alloys, cadmium telluride, or copper indium diselenide, are particularly promising because they are both well suited to mass production techniques and the amounts of active materials required are small.

Because of these merits, photovoltaics are traditionally applied in areas that are remote from utility grids, especially where the supply of power from conventional sources is impractical or costly, such as for telecommunication and weather stations. However, with falling costs and government incentives, PV has become an economic source of grid electricity in many places and the great majority of PV systems are now grid connected. These market conditions have also spurred large commercial PV systems on flat building rooftops and utility power plants. The largest plants are now in the order of hundreds of MW (RENI, 2012). For grid-connected distributed systems, the actual value of photovoltaic electricity can be high because this electricity is produced during periods of peak demand, thereby reducing the need for costly extra conventional capacity to cover the peak demand. Additionally, PV electricity is close to the sites where it is consumed, thereby reducing transmission and distribution losses and thus increasing system reliability.

Photovoltaic devices, or cells, are used to convert solar radiation directly into electricity. A review of possible materials that can be used for PV cells is given in Chapter 1, Section 1.5.1. Photovoltaic cells are made of various semiconductors, which are materials that are only moderately good conductors of electricity. The materials most commonly used are silicon (Si) and compounds of cadmium sulfide (CdS), cuprous sulfide (Cu_2S), and gallium arsenide (GaAs). These cells are packed into modules that produce a specific voltage and current when illuminated. A comprehensive review of cell and module technologies is given by Kazmerski (1997). PV modules can be connected in series or parallel to produce larger voltages or currents. PV systems rely on sunlight, have no moving parts, are

modular to match power requirements on any scale, are reliable, and have a long life. The systems can be used independently or in conjunction with other electrical power sources. Applications powered by PV systems include communications (both on earth and in space), remote power, remote monitoring, lighting, water pumping, and battery charging. Some of these applications are analyzed in Section 9.4.

9.1 Semiconductors

To understand the photovoltaic effect, some basic theory about semiconductors and their use as photovoltaic energy conversion devices needs to be given as well as information on p–n junctions. These are explained in the following sections.

As is well known, an atom consists of the nucleus and electrons that orbit the nucleus. According to quantum mechanics, electrons of an isolated atom can have only specific discrete or quantized energy levels. In elements that have electrons in multiple orbitals, the innermost electrons have the minimum (maximum negative) energy and therefore require a large amount of energy to overcome the attraction of the nucleus and become free. When atoms are brought close together, the electronic energy of individual atoms is altered and the energy levels are grouped in energy bands. In some energy bands, electrons are allowed to exist, and in other bands electrons are forbidden. The electrons at the outermost shell are the only ones that interact with other atoms. This is the highest normally filled band, which corresponds to the ground state of the valence electrons in an atom and is called the *valence band*. The electrons in the valence band are loosely attached to the nucleus of the atom and, therefore, may attach more easily to a neighboring atom, giving that atom a negative charge and leaving the original atom as a positive charged ion. Some electrons in the valence band may possess a lot of energy, which enables them to jump into a higher band. These electrons are responsible for the conduction of electricity and heat, and this band is called the *conduction band*. The difference in the energy of an electron in the valence band and the innermost shell of the conduction band is called the *band gap*.

A schematic representation of the energy band diagrams of three types of materials is shown in Figure 9.1. Materials whose valence gap is full and whose conduction band is empty have very high band gaps and are called *insulators* because no current can be carried by electrons in the filled band and the energy gap is so large that, under ordinary circumstances, a valence electron cannot accept energy, since the empty states in the conduction band are inaccessible to it. The band gap in these materials is greater than 3 eV.

Materials that have relatively empty valence bands and may have some electrons in the conduction band are called *conductors*. In this case, the valence and the conduction bands overlap. The valence electrons are able to accept energy from an external field and move to an unoccupied allowed state at slightly higher energy levels within the same band. Metals fall in this category, and the valence electrons in a metal can be easily emitted outside the atomic structure and become free to conduct electricity.

Materials with valence gaps partly filled have intermediate band gaps and are called *semiconductors*. The band gap in these materials is smaller than 3 eV. They have the same band structure as the insulators but their energy gap is much narrower. The two types of semiconductors are the pure ones, called *intrinsic semiconductors*, and those doped with small amounts of impurities, called *extrinsic semiconductors*. In intrinsic semiconductors, the valence electrons can easily be excited by

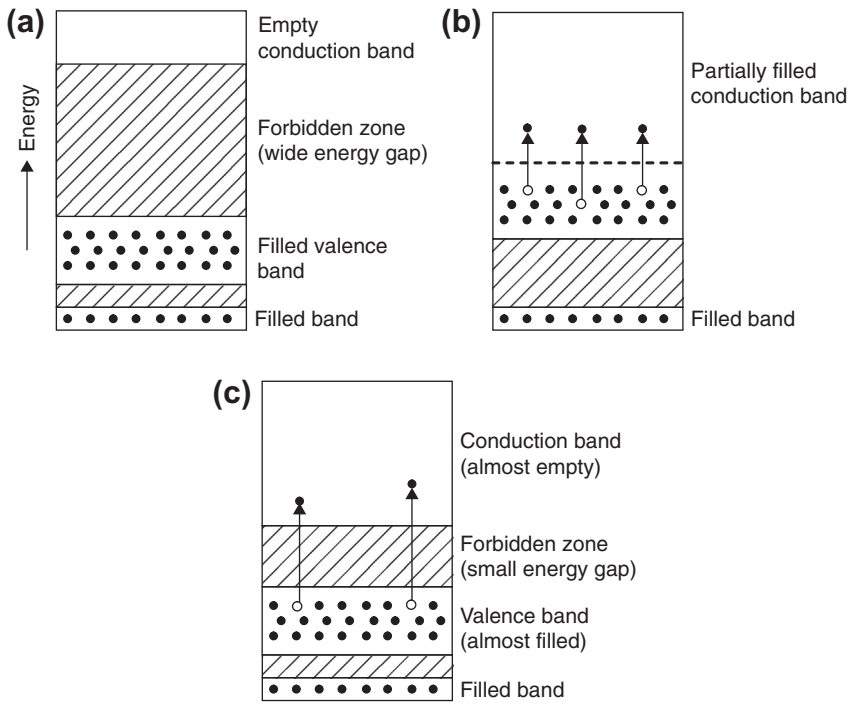

FIGURE 9.1

Schematic diagrams of energy bands for typical materials. (a) Insulator. (b) Conductor (metal). (c) Semiconductor.

thermal or optical means and jump the narrow energy gap into the conduction band, where the electrons have no atomic bonding and therefore are able to move freely through the crystal.

9.1.1 p–n Junction

Silicon (Si) belongs to group 4 of the periodic table of elements. In semiconductors, if the material that is doped has more electrons in the valence gap than the semiconductor, the doped material is called an *n-type semiconductor*. The n-type semiconductor is electronically neutral but has excess electrons, which are available for conduction. This is obtained when Si atoms are replaced with periodic table group 5 elements, such as arsenic (As) or antimony (Sb), and in so doing, form electrons that can move around the crystal. If these excess electrons are removed, the atoms will be left with positive charges.

In semiconductors, if the material that is doped has fewer electrons in the valence gap than the semiconductor, the doped material is called a *p-type semiconductor*. The p-type semiconductor is electronically neutral but it has positive holes (missing electrons) in its structure, which can accommodate excess electrons. This type of material is obtained when Si atoms are replaced with periodic table group 3 elements, such as gallium (Ga) or indium (In), and thereby form positive particles, called

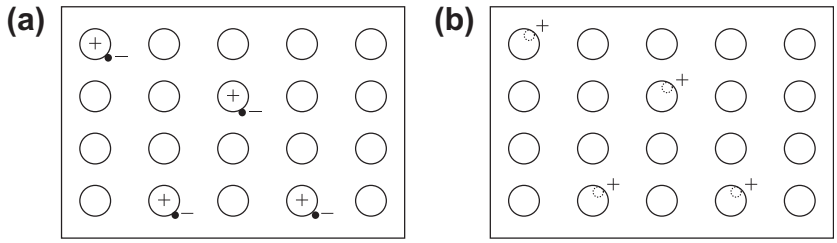

FIGURE 9.2

Schematic diagrams of n- and p-type semiconductors. (a) n-type, with excess electrons. (b) p-type, with excess positive holes.

holes, that can move around the crystal through diffusion or drift. If additional electrons could fill the holes, the impurity atoms would fit more uniformly in the structure formed by the main semiconductor atoms, but the atoms would be negatively charged.

Both types of semiconductors are shown schematically in Figure 9.2. Both n- and p-type semiconductors allow the electrons and holes to move more easily in the semiconductors. For silicon, the energy needed to get an electron across a p–n junction is 1.11 eV. This is different for each semiconductor material.

What is described in the previous paragraph occurs when the p- and n-type semiconductors are joined together, i.e., form a junction, as shown in Figure 9.3. As can be seen, when the two materials are joined, the excess electrons from the n-type jump to fill the holes in the p-type, and the holes from the p-type diffuse to the n-type side, leaving the n-side of the junction positively charged and the p-side negatively charged. The negative charges of the p-side restrict the movements of additional electrons from the n-side; however, the movement of additional electrons from the p-side is easier because of the positive charges at the junction on the n-side. Therefore the p–n junction behaves like a diode.

A schematic diagram of the energy bands of the n- and p-type semiconductors is shown in Figure 9.4. In the n-type semiconductor, because the doped impurity donates additional electrons for the conduction of current, it is called the *donor* and its energy level is called the *donor level*. The n-type energy band diagram is shown in Figure 9.4(a), and as can be seen, the donor level is located within the forbidden band. In the p-type semiconductor, the doped impurity accepts additional

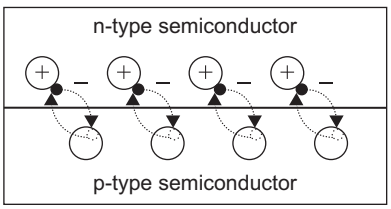

FIGURE 9.3

Schematic diagram of a p–n junction.

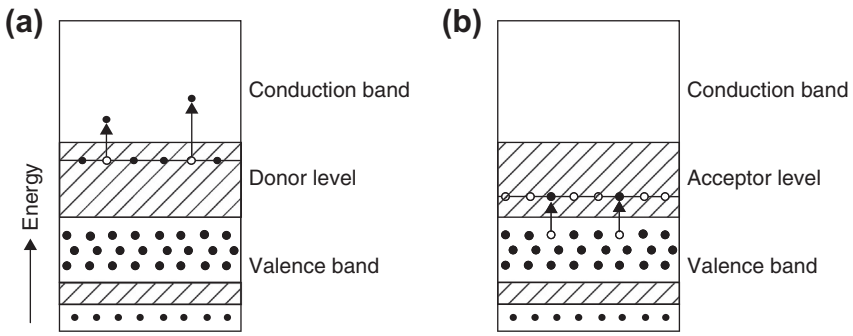

FIGURE 9.4

Energy band diagrams of n- and p-type semiconductors. (a) n-type semiconductor. (b) p-type semiconductor.

electrons; therefore, it is called the *acceptor* and its energy level is called the *acceptor level*. Its energy band diagram is shown in Figure 9.4(b), and as can be seen, the acceptor level is located in the forbidden band.

9.1.2 Photovoltaic effect

When a photon enters a photovoltaic material, it can be reflected, absorbed, or transmitted through. When this photon is absorbed by a valence electron of an atom, the energy of the electron is increased by the amount of energy of the photon. If, now, the energy of the photon is greater than the band gab of the semiconductor, the electron, which has excess energy, will jump into the conduction band, where it can move freely. Therefore, when the photon is absorbed, an electron is knocked loose from the atom. The electron can be removed by an electric field across the front and back of the photovoltaic material, and this is achieved with the help of a p–n junction. In the absence of a field, the electron recombines with the atom; whereas when there is a field, it flows through, thus creating a current. If the photon energy is smaller than that of the band gap, the electron will not have sufficient energy to jump into the conduction band, and the excess energy is converted into kinetic energy of the electrons, which leads to increased temperature. It should be noted that, irrespective of the intensity of the photon energy relative to the band gap energy, only one electron can be freed. This is the reason for the low efficiency of the photovoltaic cells.

The operation of a photovoltaic cell is shown in Figure 9.5. These solar cells contain a junction of a p-type and an n-type semiconductor, i.e., a p–n junction. To some extent, electrons and holes diffuse across the boundary of this junction, setting up an electric field across it. The free electrons are generated in the n-layer by the action of the photons. When photons of sunlight strike the surface of a solar cell and are absorbed by the semiconductor, some of them create pairs of electrons and holes. If these pairs are sufficiently near the p–n junction, its electric field causes the charges to separate, electrons moving to the n-type side and holes to the p-type side. If the two sides of the solar cell are now connected through a load, an electric current will flow as long as sunlight strikes the cell.

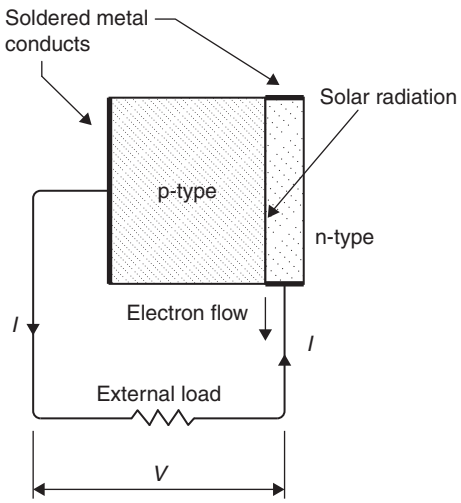

FIGURE 9.5

Photovoltaic effect.

The thickness of the n-type layer in a typical crystalline silicon cell is about 0.5 μm, whereas that of the p-type layer is about 0.25 mm. The speed of electromagnetic radiation is given by Eq. (2.31). The energy contained in a photon, E_P, is given by:

$$E_p = h\nu \tag{9.1}$$

where

h = Planck's constant, $= 6.625 \times 10^{-34}$ J s.
ν = frequency (s^{-1}).

Combining Eq. (2.31) with (9.1), we get:

$$E_p = \frac{hC}{\lambda} \tag{9.2}$$

Silicon has a band gab of 1.11 eV ($1\ \text{eV} = 1.6 \times 10^{-19}$ J); therefore, by using Eq. (9.2), it can be found that photons with wavelength of 1.12 μm or less are useful in creating electron–hole pairs and thus electricity. By checking this wavelength on the distribution shown in Figure 2.26, it can be seen that the majority of solar radiation can be used effectively in PVs. The number of photons, n_p, incident on a cell can be estimated from the intensity of light, I_p:

$$n_p = \frac{I_p}{E_p} \tag{9.3}$$

EXAMPLE 9.1

A beam of light with intensity of 3 mW and a wavelength of 743 nm is striking a solar cell. Estimate the number of photons incident on the cell.

Solution

Using Eq. (9.2) and speed of light equal to 300,000 [$= 3 \times 10^8$ m/s],

$$E_p = \frac{hC}{\lambda} = \frac{6.625 \times 10^{-34} \times 3 \times 10^8}{743 \times 10^{-9}} = 2.675 \times 10^{-19} \text{ J}$$

Using Eq. (9.3) for the intensity of 3×10^{-3} W or 3×10^{-3} J/s,

$$n_p = \frac{I_p}{E_p} = \frac{3 \times 10^{-3}}{2.675 \times 10^{-19}} = 1.12 \times 10^{16} \text{ photons/s}$$

A photovoltaic cell consists of the active photovoltaic material, metal grids, antireflection coatings, and supporting material. The complete cell is optimized to maximize both the amount of sunlight entering the cell and the power out of the cell. The photovoltaic material can be one of a number of compounds. The metal grids enhance the current collection from the front and back of the solar cell. The antireflection coating is applied to the top of the cell to maximize the light going into the cell. Typically, this coating is a single layer optimized for sunlight. As a result, photovoltaic cells range in color from black to blue. In some types of photovoltaic cells, the top of the cell is covered by a semi-transparent conductor that functions as both the current collector and the antireflection coating. A complete photovoltaic cell is a two-terminal device with positive and negative leads.

Silicon is an abundant chemical element covering 25% of the earth's crust. Silicon minerals are cheap, but silicon cells still must be individually fabricated by a long, complicated process that includes purifying the silicon, pulling a long crystal from a high-temperature melt, slicing the crystal into wafers, diffusing impurities into the wafers, and applying various coatings and electrical conducts. Labor now accounts for almost all the cost of a silicon cell. It is expected that fabrication techniques plus automation of the manufacturing process will radically lower the price within the next few years.

9.1.3 PV cell characteristics

A photovoltaic PV generator is mainly an assembly of solar cells, connections, protective parts, and supports. As was seen already, solar cells are made of semiconductor materials, usually silicon, and are specially treated to form an electric field with positive on one side (backside) and negative on the other side (front side facing the sun). When solar energy (photons) hits the solar cell, electrons are knocked loose from the atoms in the semiconductor material, creating electron–hole pairs. If electrical conductors are attached to the positive and negative sides, forming an electrical circuit, the electrons are captured in the form of electric current, called *photocurrent*, I_{ph}. As can be understood from this description, during darkness the solar cell is not active and works as a diode, i.e., a p–n junction that does not produce any current or voltage. If, however, it is connected to an external, large voltage supply, it generates a current, called the *diode* or *dark current*, I_D. A solar cell is usually represented by an electrical equivalent one-diode model, shown in Figure 9.6 (Lorenzo, 1994). This circuit can be

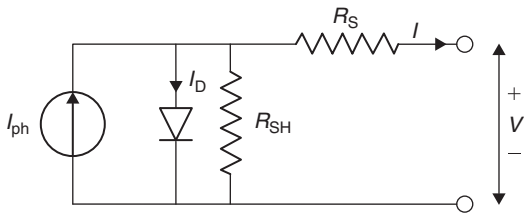

FIGURE 9.6

Single solar cell model.

used for an individual cell, a module consisting of a number of cells, or an array consisting of several modules.

As shown in Figure 9.6, the model contains a current source, I_{ph}, one diode, and a series resistance R_S, which represents the resistance inside each cell. The diode has also an internal shunt resistance, as shown in Figure 9.6. The net current is the difference between the photocurrent, I_{ph}, and the normal diode current, I_D, given by:

$$I = I_{ph} - I_D = I_{ph} - I_o\left\{\exp\left[\frac{e(V + IR_S)}{kT_C}\right] - 1\right\} - \frac{V + IR_S}{R_{SH}} \tag{9.4a}$$

It should be noted that the shunt resistance is usually much bigger than a load resistance, whereas the series resistance is much smaller than a load resistance, so that less power is dissipated internally within the cell. Therefore, by ignoring these two resistances, the net current is the difference between the photocurrent, I_{ph}, and the normal diode current, I_D, given by:

$$I = I_{ph} - I_D = I_{ph} - I_o\left[\exp\left(\frac{eV}{kT_C}\right) - 1\right] \tag{9.4b}$$

where

k = Boltzmann's gas constant, $= 1.381 \times 10^{-23}$ J/K;
T_C = absolute temperature of the cell (K);
e = electronic charge $= 1.602 \times 10^{-19}$ J/V;
V = voltage imposed across the cell (V); and
I_o = dark saturation current, which depends strongly on temperature (A).

Figure 9.7 shows the I–V characteristic curve of a solar cell for a certain irradiance (G_t) at a fixed cell temperature, T_C. The current from a PV cell depends on the external voltage applied and the amount of sunlight on the cell. When the cell is short-circuited, the current is at maximum (short-circuit current, I_{sc}), and the voltage across the cell is 0. When the PV cell circuit is open, with the leads not making a circuit, the voltage is at its maximum (open-circuit voltage, V_{oc}), and the current is 0. In either case, at open circuit or short circuit, the power (current times voltage) is 0. Between an open circuit and a short circuit, the power output is greater than 0. The typical current voltage curve shown in Figure 9.7 presents the range of combinations of current and voltage. In this representation, a sign convention is used, which takes as positive the current generated by the cell when the sun is shining and a positive voltage is applied on the cell's terminals.

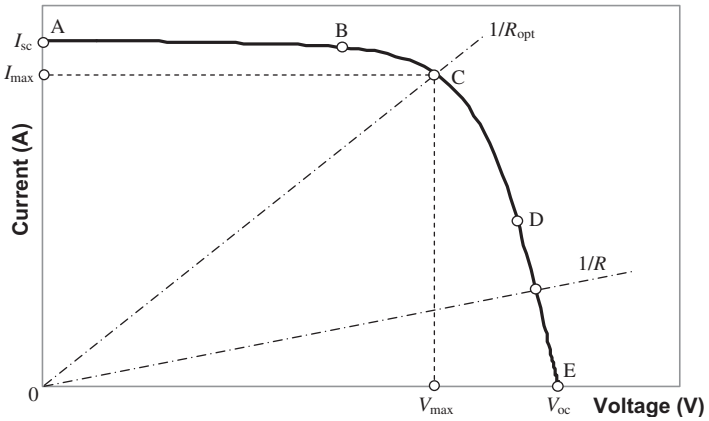

FIGURE 9.7

Representative current–voltage curve for photovoltaic cells.

If the cell's terminals are connected to a variable resistance, R, the operating point is determined by the intersection of the I–V characteristic of the solar cell with the load I–V characteristics. As shown in Figure 9.7 for a resistive load, the load characteristic is a straight line with a slope $1/V = 1/R$. If the load resistance is small, the cell operates in the region AB of the curve, where the cell behaves as a constant current source, almost equal to the short-circuit current. On the other hand, if the load resistance is large, the cell operates on the region DE of the curve, where the cell behaves more as a constant voltage source, almost equal to the open-circuit voltage. The power can be calculated by the product of the current and voltage. If this exercise is performed and the results are plotted on a P–V graph, then Figure 9.8 can be obtained. The maximum power passes from a maximum power point (point C on

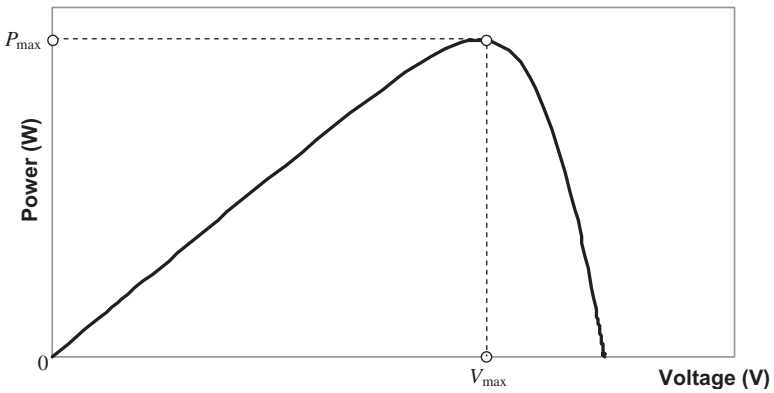

FIGURE 9.8

Representative power–voltage curve for photovoltaic cells.

Figure 9.7), at which point the load resistance is optimum, R_{opt}, and the power dissipated in the resistive load is maximum and given by:

$$P_{max} = I_{max} V_{max} \tag{9.5}$$

Point C on Figure 9.7 is also called the *maximum power point*, which is the operating point P_{max}, I_{max}, V_{max} at which the output power is maximized. Given P_{max}, an additional parameter, called the *fill factor*, FF, can be calculated such that:

$$P_{max} = I_{sc} V_{oc} \text{FF} \tag{9.6}$$

or

$$\text{FF} = \frac{P_{max}}{I_{sc} V_{oc}} = \frac{I_{max} V_{max}}{I_{sc} V_{oc}} \tag{9.7}$$

The fill factor is a measure of the real I–V characteristic. For good cells, its value is greater than 0.7. The fill factor decreases as the cell temperature increases.

Thus, by illuminating and loading a PV cell so that the voltage equals the PV cell's V_{max}, the output power is maximized. The cell can be loaded using resistive loads, electronic loads, or batteries. Typical parameters of a single-crystal solar cell are current density $I_{sc} = 32$ mA/cm^2, $V_{oc} = 0.58$ V, $V_{max} = 0.47$ V, FF $= 0.72$, and $P_{max} = 2273$ mW (ASHRAE, 2004).

Other fundamental parameters that can be obtained from Figure 9.7 are the short-circuit current and the open-circuit voltage. The short-circuit current, I_{sc}, is the higher value of the current generated by the cell and is obtained under short-circuit conditions, i.e., $V = 0$, and is equal to I_{ph}. The open-circuit voltage corresponds to the voltage drop across the diode when it is traversed by the photocurrent, I_{ph}, which is equal to I_D, when the generated current is $I = 0$. This is the voltage of the cell during nighttime and can be obtained from Eq. (9.4b):

$$\exp\left(\frac{eV_{oc}}{kT_C}\right) - 1 = \frac{I_{sc}}{I_o} \tag{9.8}$$

which can be solved for V_{oc}:

$$V_{oc} = \frac{kT_C}{e} \ln\left(\frac{I_{sc}}{I_o} + 1\right) = V_t \ln\left(\frac{I_{sc}}{I_o} + 1\right) \tag{9.9}$$

where V_t = thermal voltage (V) given by:

$$V_t = \frac{kT_C}{e} \tag{9.10}$$

The output power, P, from a photovoltaic cell is given by:

$$P = IV \tag{9.11}$$

The output power depends also on the load resistance, R; and by considering that $V = IR$, it gives:

$$P = I^2 R \tag{9.12}$$

Substituting Eq. (9.4b) into Eq. (9.11) gives:

$$P = \left\{ I_{sc} - I_o \left[\exp\left(\frac{eV}{kT_C} \right) - 1 \right] \right\} V \tag{9.13}$$

Equation (9.13) can be differentiated with respect to V. By setting the derivative equal to 0, the external voltage, V_{max}, that gives the maximum cell output power can be obtained:

$$\exp\left(\frac{eV_{max}}{kT_C} \right) \left(1 + \frac{eV_{max}}{kT_C} \right) = 1 + \frac{I_{sc}}{I_o} \tag{9.14}$$

This is an explicit equation of the voltage V_{max}, which maximizes the power in terms of the short-circuit current ($I_{sc} = I_{ph}$), the dark saturation current (I_o), and the absolute cell temperature, T_C. If the values of these three parameters are known, then V_{max} can be obtained from Eq. (9.14) by trial and error.

The load current, I_{max}, which maximizes the output power, can be found by substituting Eq. (9.14) into Eq. (9.4b):

$$I_{max} = I_{sc} - I_o \left[\exp\left(\frac{eV}{kT_C} \right) - 1 \right] = I_{sc} - I_o \left[\frac{1 + \frac{I_{sc}}{I_o}}{1 + \frac{eV_{max}}{kT_C}} - 1 \right] \tag{9.15}$$

which gives:

$$I_{max} = \frac{eV_{max}}{kT_C + eV_{max}} (I_{sc} + I_o) \tag{9.16}$$

By using Eq. (9.5),

$$P_{max} = \frac{eV_{max}^2}{kT_C + eV_{max}} (I_{sc} + I_o) \tag{9.17}$$

Efficiency is another measure of PV cells that is sometimes reported. *Efficiency* is defined as the maximum electrical power output divided by the incident light power. Efficiency is commonly reported for a PV cell temperature of 25 °C and incident light at an irradiance of 1000 W/m^2 with a spectrum close to that of sunlight at solar noon. An improvement in cell efficiency is directly connected to a cost reduction in photovoltaic systems. A series of R&D efforts have been made on each step of the photovoltaic process. Through this technological progress, the efficiency of a single crystalline silicon solar cell reaches 14–15% and the polycrystalline silicon solar cells shows 12–13% efficiency in the mass production lines.

Another parameter of interest is the maximum efficiency, which is the ratio between the maximum power and the incident light power, given by:

$$\eta_{max} = \frac{P_{max}}{P_{in}} = \frac{I_{max} V_{max}}{AG_t} \tag{9.18}$$

where

A = cell area (m^2).

EXAMPLE 9.2

If the dark saturation current of a solar cell is 1.7×10^{-8} A/m^2, the cell temperature is 27 °C, and the short-circuit current density is 250 A/m^2, calculate the open-circuit voltage, V_{oc}; voltage at maximum power, V_{max}; current density at maximum power, I_{max}; maximum power, P_{max}; and maximum efficiency, η_{max}. What cell area is required to get an output of 20 W when the available solar radiation is 820 W/m^2?

Solution

First the value of e/kT_C is evaluated, which is used in many relations:

$$\frac{e}{kT_C} = \frac{1.602 \times 10^{-19}}{1.381 \times 10^{-23} \times 300} = 38.67 \text{ V}^{-1}$$

Using Eq. (9.9),

$$V_{oc} = \frac{kT_C}{e} \ln\left(\frac{I_{sc}}{I_o} + 1\right) = \frac{1}{38.67} \ln\left(\frac{250}{1.7 \times 10^{-8}} + 1\right) = 0.605 \text{ V}$$

Voltage at maximum power can be found from Eq. (9.14) by trial and error:

$$\exp\left(\frac{eV_{max}}{kT_C}\right)\left(1 + \frac{eV_{max}}{kT_C}\right) = 1 + \frac{I_{sc}}{I_o}$$

or

$$\exp(38.67V_{max})(1 + 38.67V_{max}) = 1 + \frac{250}{1.7 \times 10^{-8}}$$

which gives $V_{max} = 0.526$ V.

The current density at maximum power point can be estimated from Eq. (9.16):

$$I_{max} = \frac{eV_{max}}{kT_C + eV_{max}}(I_{sc} + I_o)$$

$$= \frac{1.602 \times 10^{-19} \times 0.526}{1.381 \times 10^{-23} \times 300 + 1.602 \times 10^{-19} \times 0.526}\left(250 + 1.7 \times 10^{-8}\right) = 238.3 \text{ A/m}^2$$

Maximum power, P_{max}, is obtained from Eq. (9.5):

$$P_{max} = I_{max}V_{max} = 238.3 \times 0.526 = 125.3 \text{ W/m}^2$$

Maximum efficiency, η_{max}, is obtained from Eq. (9.18):

$$\eta_{max} = \frac{P_{max}}{P_{in}} = \frac{125.3}{820} = 15.3\%$$

Finally, the cell area required to get an output of 20 W is:

$$A = \frac{P_{req}}{P_{max}} = \frac{20}{125.3} = 0.16 \text{ m}^2$$

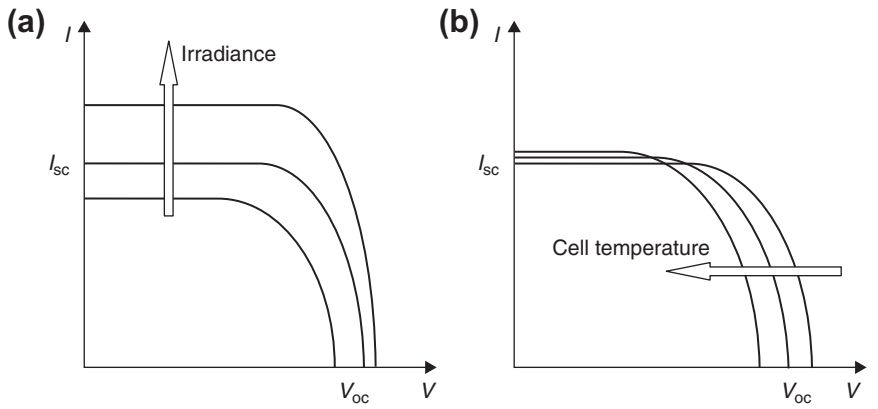

FIGURE 9.9

Influence of irradiation and cell temperature on PV cell characteristics. (a) Effect of increased irradiation. (b) Effect of increased cell temperature.

The *I–V* characteristic of the solar cell, presented in Figure 9.7, is only for a certain irradiance, G_t, and cell temperature, T_C. The influences of these two parameters on the cell characteristics are shown in Figure 9.9. As shown in Figure 9.9(a), the open-circuit voltage increases logarithmically by increasing the solar radiation, whereas the short-circuit current increases linearly. The influence of the cell temperature on the cell characteristics is shown in Figure 9.9(b). The main effect of the increase in cell temperature is on open-circuit voltage, which decreases linearly with the cell temperature; thus the cell efficiency drops. As can be seen, the short-circuit current increases slightly with the increase of the cell temperature.

In practice solar cells can be connected in series or parallel. Figure 9.10 shows how the *I–V* curve is modified in the case where two identical cells are connected in parallel and in series. As can be seen,

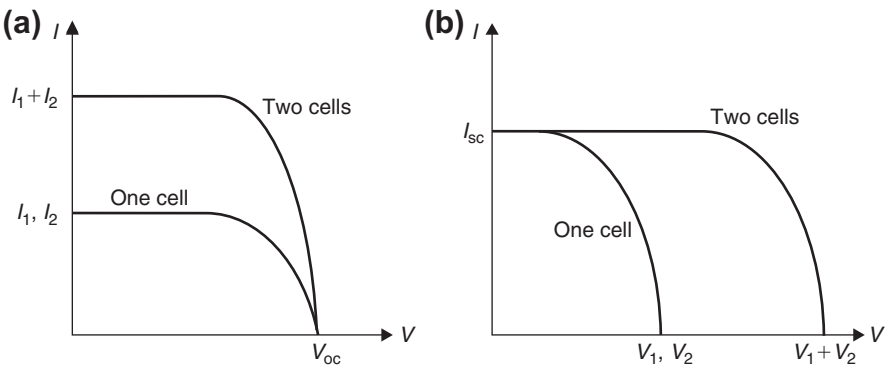

FIGURE 9.10

Parallel and series connection of two identical solar cells. (a) Parallel connection. (b) Series connection.

when two identical cells are connected in parallel, the voltage remains the same but the current is doubled; when the cells are connected in series, the current remains the same but the voltage is doubled.

9.2 Photovoltaic panels

PV modules are designed for outdoor use in such harsh conditions as marine, tropic, arctic, and desert environments. The choice of the photovoltaically active material can have important effects on system design and performance. Both the composition of the material and its atomic structure are influential. Photovoltaic materials include silicon, gallium arsenide, copper indium diselenide, cadmium telluride, indium phosphide, and many others. The atomic structure of a PV cell can be a single crystal, polycrystalline, or amorphous. The most commonly produced PV material is crystalline silicon, either single crystal or polycrystalline.

Cells are normally grouped into modules, which are encapsulated with various materials in order to protect the cells and the electrical connectors from the environment (Hansen et al., 2000). As shown in Figure 9.11, PV cell modules consist of N_{PM} parallel branches and each branch has N_{SM} solar cells in series. In the following analysis, superscript M refers to the PV module and superscript C refers to the solar cell. Therefore, as shown in Figure 9.11, the applied voltage at the module's terminals is denoted by V^M, whereas the total generated current is denoted by I^M.

A model of the PV module can be obtained by replacing each cell in Figure 9.11 with the equivalent diagram from Figure 9.6. The model, developed by Lorenzo (1994), has the advantage that it can be used by applying only standard manufacturer-supplied data for the modules and the cells. The PV module current I^M under arbitrary operating conditions can be described by:

$$I^M = I_{sc}^M \left[1 - \exp\left(\frac{V^M - V_{oc}^M + R_S^M I^M}{N_{SM} V_t^C} \right) \right] \tag{9.19}$$

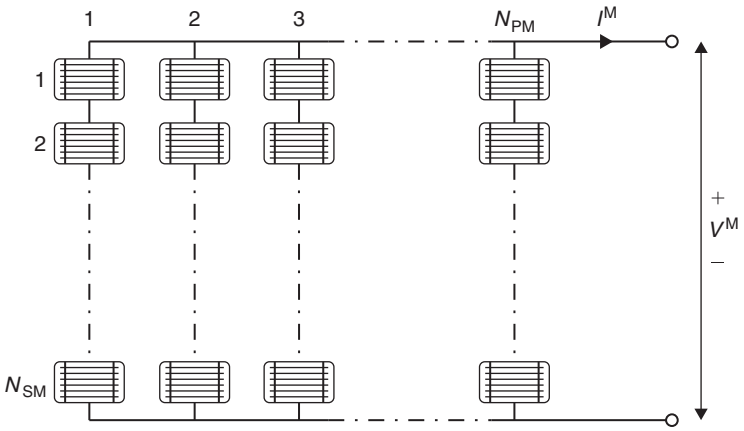

FIGURE 9.11

Schematic diagram of a PV module consisting of N_{PM} parallel branches, each with N_{SM} cells in series.

Table 9.1 SRC and NOCT Conditions

SRC Conditions	NOCT Conditions
Irradiation: $G_{t,o} = 1000\,W/m^2$ Cell temperature: $T_o^C = 25°C$	Irradiation: $G_{t,NOCT} = 800\,W/m^2$ Ambient temperature: $T_{a,NOCT} = 20\,°C$ Wind speed: $W_{NOCT} = 1\,m/s$

It should be noted that the PV module current, I^M, is an implicit function, which depends on:

1. The short-circuit current of the module, given by:

$$I_{sc}^M = N_{PM} I_{sc}^C$$

2. The open-circuit voltage of the module, given by:

$$V_{oc}^M = N_{PM} V_{oc}^C$$

3. The equivalent series resistance of the module, given by:

$$R_S^M = \frac{N_{SM}}{N_{PM}} R_S^C$$

4. The thermal voltage in the semiconductor of a single solar cell, given by:

$$V_t^C = \frac{kT^C}{e}$$

The current practice dictates that the performance of a PV module is determined by exposing it at known standard rating conditions (SRCs) of irradiance, $G_{t,o} = 1000\,W/m^2$, and cell temperature, $T_o^C = 25\,°C$. These conditions are different from the nominal operating cell temperature (NOCT), as indicated in Table 9.1.

9.2.1 PV arrays

The modules in a PV system are usually connected in arrays. An array with M_P parallel branches each with M_S modules in series is shown in Figure 9.12. By using a superscript A to denote array characteristics, the applied voltage at the array's terminals is donated V^A, whereas the total current of the array is denoted I^A, given by:

$$I^A = \sum_{i=1}^{M_P} I_i \tag{9.20}$$

If it is assumed that the modules are identical and the ambient irradiance is the same in all modules, then the array's current is given by:

$$I^A = M_p I^M \tag{9.21}$$

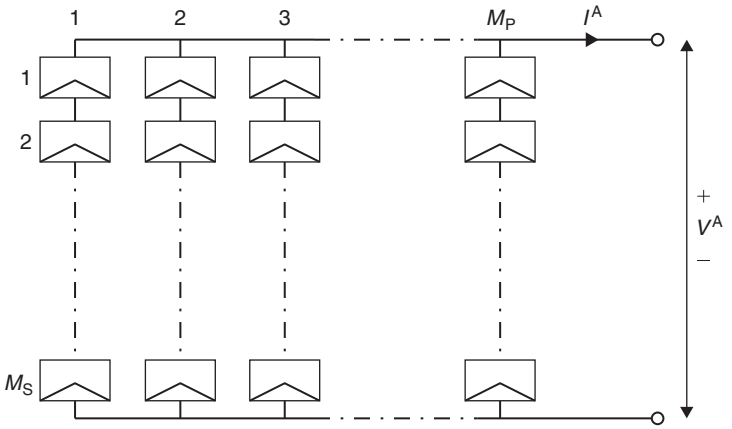

FIGURE 9.12

Cell array consisting of M_P parallel branches, each with M_S modules in series.

EXAMPLE 9.3

A PV system is required to produce 250 W at 24 V. Using the solar cells of Example 9.2, design the PV panel, working at the maximum power point, if each cell is 9 cm^2 in area.

Solution

From Example 9.2, $V_{max} = 0.526$ V. The current density at maximum power point is 238.3 A/m^2. Therefore, for the current cell,

$$I_{max} = 238.3 \times 9 \times 10^{-4} = 0.2145 \text{ A}$$

This yields a power per cell $= 0.526 \times 0.2145 = 0.1$ W.
Number of cells required $= 250/0.1 = 2500$.
Number of cells in series = system voltage/voltage per cell $= 24/0.526 = 45.6 \approx 46$ (in fact with 46 cells, Voltage = 24.2 V).
Number of rows of 46 cells each, connected in parallel $= 2500/46 = 54.3 \approx 55$ (in fact this panel yields $55 \times 46 \times 0.1 = 253$ W).

PV cells are fragile and susceptible to corrosion by humidity or fingerprints and can have delicate wire leads. Also, the operating voltage of a single PV cell is about 0.5 V, making it unusable for many applications. A *module* is a collection of PV cells that provides a usable operating voltage and offers means that protects the cells. Depending on the manufacturer and the type of PV material, modules have different appearances and performance characteristics. Also, modules may be designed for specific conditions, such as hot and humid, desert, or frozen climates. Usually, the cells are series connected to other cells to produce an operating voltage around 30–60 V. These strings of cells are then encapsulated with a polymer, a front glass cover, and a back material. Also, a junction box is attached at the back of the module for convenient wiring to other modules or other electrical equipment.

9.2.2 Types of PV technology

Many types of PV cells are available today. The main types are crystalline silicon, which accounts for roughly 80% of the PV market; thin-films, which have expanded to around 20% market share; and triple-junction cells, which are used in the emerging field of concentrating PV. This section gives details of commercialized flat-plate PV technologies and an overview of the cells that are currently in the research and development stage. Concentrating PV is discussed in section 9.7.

The choice between crystalline or thin-film PV modules for a given project depends heavily on climate and space. As we shall see below, crystalline modules are more efficient (i.e., give greater power output per unit area of module), while thin-film modules tend to have higher yield (i.e., give greater energy production for a given power rating)—especially in high temperatures (RENI, 2012). Assuming the same module price ($/W), crystalline modules are thus suited to space-constrained projects in moderate climates, and thin-film to hot climates and abundant space.

- *Monocrystalline silicon cells.* These cells are made from pure monocrystalline silicon. In these cells, the silicon has a single continuous crystal lattice structure with almost no defects or impurities. The main advantage of monocrystalline cells is their high efficiency, which is typically around 14–15%. Premium modules are available in the market with efficiencies just over 20% (RENI, 2012).

  A disadvantage of these cells is the complicated manufacturing process that leads to relatively high costs, although greater production capacity of its raw material has decreased its price markedly in recent years, making it (and multicrystalline silicon) more price-competitive with thin-film modules. Compared to thin-film technologies, the power output of crystalline silicon decreases more rapidly with increasing cell temperature—its temperature coefficient is around minus 0.4–0.5%/°C. Additionally, the efficiency of crystalline silicon decreases somewhat in low light conditions, whereas the efficiency of thin-film modules remains roughly constant (Marion, 2008). Being relatively expensive, monocrystalline modules are most often used where the most possible power is required from a confined space, such as residential and commercial rooftops.
- *Multicrystalline silicon cells.* Multicrystalline cells, also known as polycrystalline cells, are produced using numerous grains of monocrystalline silicon. In the manufacturing process, molten polycrystalline silicon is cast into ingots, which are subsequently cut into very thin wafers and assembled into complete cells. Multicrystalline cells are cheaper to produce than monocrystalline ones because of the simpler manufacturing process required. They are, however, slightly less efficient, with typical module efficiencies around 13–15% (Price and Margolis, 2010) and high-end products up to 17% (RENI, 2010). They share monocrystalline cells' relatively high temperature coefficient. With a long track record, high efficiency and moderate cost, multicrystalline modules are widely used in a wide variety of applications including roof- and ground-mounted arrays.
- *Amorphous silicon.* The general characteristics of amorphous silicon solar cells are given in Chapter 1, Section 1.5.1. Unlike mono- and multicrystalline cells, the silicon atoms in amorphous silicon (a-Si) cells are arranged in a thin homogenous layer. Amorphous silicon absorbs light more effectively than crystalline silicon, which leads to thinner cells, giving rise to the name *thin film* photovoltaics.

Advantages of these cells are their low manufacturing cost and high energy production per rated power capacity (kWh/kWp). The high yield stems from two attributes (Jardine et al., 2001; Kullmann, 2009):

1. Of all mass-market PV technologies, a-Si is the least impacted by heat, with a temperature coefficient of only around -0.2%/°C (Marion, 2008).
2. Amorphous silicon is relatively effective at absorbing the blue wavelengths of light that are encountered in cloudy conditions. Thus over the course of a year a-Si modules will generally produce more electricity than crystalline silicon ones of the same peak power, especially in warm climates.

The efficiency of a-Si modules is only 6–7% (Price and Margolis, 2010). Because of their low cost they are applied in a wide variety of PV systems; however, they face increasing competition from other thin-film technologies with higher efficiencies (see the following two types below). To increase their efficiency, a-Si is increasingly combined with layers of multicrystalline silicon or a variant, microcrystalline silicon. The properties of such "hybrid" modules lie between pure a-Si and crystalline silicon, with efficiencies around 9–10%. Some large PV manufacturers have phased out pure a-Si product lines and replaced them with hybrid designs. Perhaps the greatest advantage of these cells is that amorphous silicon can be deposited on a wide range of substrates, both rigid and flexible. Nowadays, the panels made from amorphous silicon solar cells come in a variety of shapes, such as roof tiles, which can replace normal ceramic tiles in a solar roof.

- *Cadmium Telluride (CdTe).* The thin-film PV market was largely developed by a single manufacturer, First Solar. It accounted for 59% of the global thin-film market in 2008 (Schreiber, 2009), as a result of achieving low cost (it was the first company to manufacture PV modules at less than $1 per Watt) and large production capacity (Runyon, 2012). Although the price advantage of CdTe has fallen with the emergence of low-cost crystalline silicon production in China, it retains a sizeable market presence with a manufacturing cost under $0.75/W (Runyon, 2012) and around 2 GW of annual production capacity.

  Like amorphous silicon, CdTe is relatively tolerant to heat (its temperature coefficient is around minus 0.25–0.35%/°C), yet it has a higher efficiency of 10–11%. This combination of low cost, moderate efficiency, and large manufacturing volume has seen CdTe help create a new market for PV in recent years, that of utility-scale solar power plants. While CdTe modules are well suited to large ground-mounted arrays for commercial electricity production, they are also deployed on commercial rooftops.
- *Copper Indium Gallium Selenide (CIGS).* The most recent thin-film technology to be commercialized is the CIGS family. Like the other thin-films it can be manufactured at low cost and high volume in a continuous (as opposed to batch) manufacturing process. CIGS is also the main candidate for the commercial development of modules that do not use glass, making them flexible and very lightweight. Their electrical properties lie between crystalline silicon and CdTe, with conversion efficiency around 10–13% and moderate temperature coefficient of minus 0.3–0.4%/°C.

  The moderate efficiency, low cost and light weight of CIGS make them ideally suited to rooftop installations, both residential and commercial. They are also a promising technology for building-integrated photovoltaic (BIPV) products. Numerous companies have been established to manufacture CIGS modules in recent years (Schreiber, 2009), although being new to the

market they have not yet been deployed at the large scale of the other above-mentioned technologies (RENI, 2010).

- *Thermophotovoltaics.* These are photovoltaic devices that, instead of sunlight, use the infrared region of radiation, i.e., thermal radiation. A complete thermophotovoltaic (TPV) system includes a fuel, a burner, a radiator, a longwave photon recovery mechanism, a PV cell, and a waste heat recuperation system (Kazmerski, 1997). TPV devices convert radiation using exactly the same principles as photovoltaic devices, outlined in previous sections. The key differences between PV and TPV conversion are the temperatures of the radiators and the system geometries. In a solar cell, the radiation is received from the sun, which is at a temperature of about 6000 K and a distance of about 150×10^6 km. A TPV device, however, receives radiation, in either the broad or narrow band, from a surface at a much lower temperature of about 1300–1800 K and a distance of only a few centimeters. Although the blackbody power radiated by a surface varies at the fourth power of the absolute temperature, the inverse square law dependence of the power received by the detectors dominates. Therefore, although the power received by a non-concentrator solar cell is on the order of 0.1 W/cm^2, that received by a TPV converter is likely to be 5–30 W/cm^2, depending on the radiator temperature. Consequently, the power density output from a TPV converter is expected to be significantly greater than that from a non-concentrator PV converter. More details on TPVs can be found in the article by Coutts (1999).

Under development are polymer and organic solar cells. The attraction of these technologies is that they potentially offer fast production at low cost in comparison to crystalline silicon technologies, yet they typically have lower efficiencies, around 5% (Price and Margolis, 2010), and despite the demonstration of operational lifetimes and dark stabilities under inert conditions for thousands of hours, they suffer from stability and degradation problems. Organic materials are attractive, primarily due to the prospect of high-output manufacture using reel-to-reel or spray deposition. Other attractive features are the possibilities for ultrathin, flexible devices, which may be integrated into appliances or building materials, and tuning of color through the chemical structure (Nelson, 2002).

Another type of device being developed is the nano-PV, considered the third-generation PV; the first generation is the crystalline silicon cells, and the second generation thin-films. Instead of conductive materials and a glass substrate, nano-PV technologies rely on coating or mixing "printable" and flexible polymer substrates with electrically conductive nano-materials. This type of photovoltaics is expected to be commercially available within the next few years, reducing tremendously the cost of PV cells.

9.3 Related equipment

Photovoltaic modules can be mounted on the ground or a building roof or can be included as part of the building structure, usually the façade. Wind and snow loading are major design considerations. The PV modules can last more than 25 years, in which case the support structures and building should be designed for at least as long as the same lifetime. Related equipment includes batteries, charge controllers, inverters, and peak-power trackers.

9.3.1 Batteries

Batteries are required in many PV systems to supply power at night or when the PV system cannot meet the demand. The selection of battery type and size depends mainly on the load and availability requirements. When batteries are used, they must be located in an area without extreme temperatures, and the space where the batteries are located must be adequately ventilated.

The main types of batteries available today include lead-acid, nickel cadmium, nickel hydride, and lithium. Deep-cycle lead-acid batteries are the most commonly used. These can be flooded or valve-regulated batteries and are commercially available in a variety of sizes. Flooded (or wet) batteries require greater maintenance but, with proper care, can last longer, whereas valve-regulated batteries require less maintenance.

The principal requirement of batteries for a PV system is that they must be able to accept repeated deep charging and discharging without damage. Although PV batteries have an appearance similar to car batteries, the latter are not designed for repeated deep discharges and should not be used. For more capacity, batteries can be arranged in parallel.

Batteries are used mainly in stand-alone PV systems to store the electrical energy produced during the hours when the PV system covers the load completely and there is excess or when there is sunshine but no load is required. During the night or during periods of low solar irradiation, the battery can supply the energy to the load. Additionally, batteries are required in such a system because of the fluctuating nature of the PV system output.

Batteries are classified by their nominal capacity ($q_{\max}$), which is the number of ampere hours (Ah) that can be maximally extracted from the battery under predetermined discharge conditions. The efficiency of a battery is the ratio of the charge extracted (Ah) during discharge divided by the amount of charge (Ah) needed to restore the initial state of charge (SOC). Therefore, the efficiency depends on the SOC and the charging and discharging current. The SOC is the ratio between the present capacity of the battery and the nominal capacity; that is,

$$\text{SOC} = \frac{q}{q_{\max}} \tag{9.22}$$

As can be understood from the preceding definition and Eq. (9.22), SOC can take values between 0 and 1. If SOC = 1, then the battery is fully charged; and if SOC = 0, then the battery is totally discharged.

Other parameters related to batteries are the charge or discharge regime and the lifetime of the battery. The charge (or discharge) regime, expressed in hours, is the parameter that reflects the relationship between the nominal capacity of a battery and the current at which it is charged (or discharged)—for example, a discharge regime is 40 h for a battery with nominal capacity of 200 Ah that is discharged at 5 A. The lifetime of the battery is the number of charge–discharge cycles the battery can sustain before losing 20% of its nominal capacity.

In general, the battery can be viewed as a voltage source, E, in series with an internal resistance, R_o, as shown in Figure 9.13. In this case, the terminal voltage, V, is given by:

$$V = E - IR_o \tag{9.23}$$

9.3.2 Inverters

An inverter is used to convert the direct current into alternating current electricity. The output of the inverter can be single or three phase. Inverters are rated by the total power capacity, which ranges from

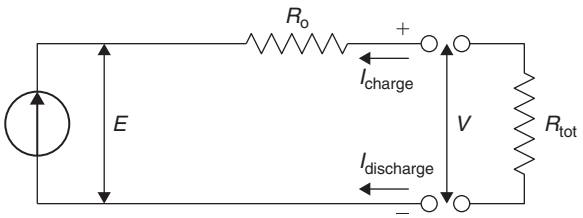

FIGURE 9.13

Schematic diagram of a battery.

hundreds of watts to megawatts. Some inverters have good surge capacity for starting motors, and others have limited surge capacity. The designer should specify both the type and size of the load the inverter is intended to service.

The inverter is characterized by a power-dependent efficiency, η_{inv}. Besides changing the DC into AC, the main function of the inverter is to keep a constant voltage on the AC side and convert the input power, P_{in}, into the output power, P_{out}, with the highest possible efficiency, given by:

$$\eta_{inv} = \frac{P_{out}}{P_{in}} = \frac{V_{ac} I_{ac} \cos(\varphi)}{V_{dc} I_{dc}} \tag{9.24}$$

where

$\cos(\varphi)$ = power factor.
I_{dc} = current required by the inverter from the DC side, i.e., controller (A); and
V_{dc} = input voltage for the inverter from the DC side, i.e., controller (V).

Numerous types of inverters are available, but not all are suitable for use when feeding power back into the mains supply.

The efficiency of an inverter depends on the fraction of its rated power at which it operates. A PV system operates at high efficiency either when it has one inverter operating with a load large enough to maintain peak efficiency or is an interconnection of module-integrated inverters or master-slave configurations (Woyte et al., 2000). When one inverter is used, this is supplied with power from several series-connected PV modules connected in parallel on a DC bus. This configuration has a low-cost and provides high efficiency but requires a complex DC installation. In a module-integrated inverter, each PV module has its own individual inverter, called *micro-inverter* (see Section 9.3.4). These are more expensive than a central inverter; however, they prevent the use of expensive DC wiring (Woyte et al., 2000). A master-slave configuration requires multiple inverters connected together and generally can give greater PV output. At low solar irradiation, all the PVs of the array are connected to just a single inverter operating the inverter at its peak input power level, when solar irradiation increases the PV array is divided progressively into smaller sets of PVs, until every inverter operates independently at or near its peak rated capacity. Module-integrated inverters are located generally at the back of each module converting its DC output to AC power.

Inverter efficiency reaches its maximum, above 90%, for an input power level usually between 30% and 50% of its rated capacity. When a PV module is shaded, the PV output current decreases

significantly, causing not only the particular module output power to drop, but the output power also drops which in turn affects inverter performance (Hashimoto et al., 2000).

The performance of an inverter depends on its point of work, threshold of operation, inverter output waveform, harmonic distortion and frequency, PV efficiency, maximum power point tracker (MPPT) and transformer (Norton et al., 2011). The main functions of an inverter are wave-shaping, regulation of output voltage, and operation near peak power point (Kjar et al., 2005). The three major types of inverter are sine wave, modified sine wave, and square wave. The major advantage of a sine wave inverter is that most appliances are designed for a sine-wave operation. A modified sine-wave inverter has a waveform more like a square wave, but with an extra step, can also operate with most appliances. Finally, a square-wave inverter can generally operate only simple devices with universal motors but its greatest advantage is that it is much cheaper than the sine-wave inverter. Additionally, using a power filter, the output square waveform can be converted to a sine waveform.

9.3.3 Charge controllers

Controllers regulate the power from PV modules to prevent the batteries from overcharging. The controller can be a shunt type or series type and also function as a low-battery voltage disconnect to prevent the battery from over-discharge. The controller is chosen for the correct capacity and desired features (ASHRAE, 2004).

Normally, controllers allow the battery voltage to determine the operating voltage of a PV system. However, the battery voltage may not be the optimum PV operating voltage. Some controllers can optimize the operating voltage of the PV modules independently of the battery voltage so that the PV operates at its maximum power point.

Any power system includes a controller and a control strategy, which describes the interactions between its components. In PV systems, the use of batteries as a storage medium implies the use of a charge controller. This is used to manage the flow of energy from PV system to batteries and load by using the battery voltage and its acceptable maximum and minimum values. Most controllers have two main modes of operation:

1. *Normal operating condition*, where the battery voltage varies between the acceptable maximum and minimum values.
2. *Over-charge or over-discharge condition*, which occurs when the battery voltage reaches a critical value.

The second mode of operation is obtained by using a switch with a hysteresis cycle, such as electromechanical or solid-state devices. The operation of this switch is shown in Figure 9.14.

As shown in Figure 9.14(a), when the terminal voltage increases above a certain threshold, $V_{max,off}$, and when the current required by the load is less than the current supplied by the PV array, the batteries are protected from excessive charge by disconnecting the PV array. The PV array is connected again when the terminal voltage decreases below a certain value, $V_{max,on}$ (Hansen et al., 2000).

Similarly, as shown in Figure 9.14(b), when the current required by the load is bigger than the current delivered by the PV array, to protect the battery against excessive discharge the load is disconnected when the terminal voltage falls below a certain threshold, $V_{min,off}$. The load is connected to the system again when the terminal voltage is above a certain threshold, $V_{min,on}$ (Hansen et al., 2000).

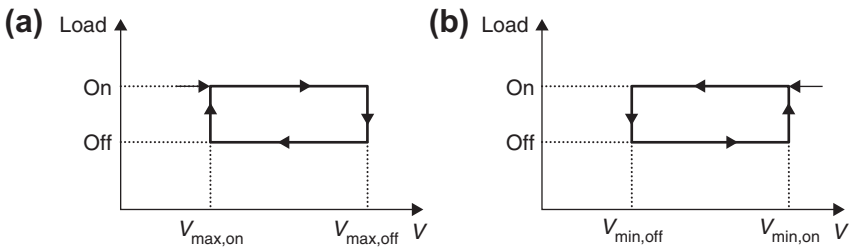

FIGURE 9.14

Operating principle of over-charge and over-discharge protection. (a) Over-charge. (b) Over-discharge.

9.3.4 Peak-power trackers

As was seen before, PV cells have a single operating point where the values of the current (I) and voltage (V) of the cell result in a maximum power output. These values correspond to a particular resistance, which is equal to V/I, as specified by Ohm's law. A PV cell has an exponential relationship between current and voltage, and there is only one optimum operating point, also called a *maximum power point* (MPP), on the power–voltage (or current) curve, as shown in Figure 9.8. MPP changes according to the radiation intensity and the cell temperature, as shown in Figure 9.9. Maximum power point trackers (MPPTs) utilize some type of control circuit or logic to search for this point and, thus, allow the converter circuit to extract the maximum power available from a cell. In fact, peak-power trackers optimize the operating voltage of a PV system to maximize the current. Typically, the PV system voltage is charged automatically. Simple peak-power trackers may have fixed operator-selected set points.

MPP trackers can either be applied at the array level or at the module level. In the former, a single tracker controls the current through all modules in the array. This function in fact is commonly integrated into the array's inverter, as already indicated in Section 9.3.2. The advantage of this approach is that a single large inverter/controller is used, which simplifies maintenance, minimizes cost, and allows high inverter efficiency. Its drawback is that the same current flows through all modules that are connected in series in the array, and because some modules may have different I–V curves than others, not all modules will operate at their individual maximum power point. This is especially problematic when inconsistent manufacturing leads to variability between modules—"module mismatch"—and when modules in an array experience different amounts of shading or soiling. Modules may also age at different rates, causing further variation in I–V curves.

To overcome this problem, MPP controllers can be applied to individual modules in an array, so that every module operates at its own maximum power point. These may either be DC–DC controllers, which still require a central inverter, or DC–AC "micro-inverters" which perform both MPP control and inversion as is seen also in Section 9.3.2. Manufacturers of both devices claim that they can increase the yield of a PV array by 5–20%. In addition, they allow malfunctioning modules in a system to be more easily identified, as the output of each module is monitored. However multiple small controllers inherently cost more than a single centralized one. Therefore, a cost/benefit analysis needs to be carried out before choosing the right system to make sure that the extra energy collected offsets the extra cost of the MPP.

Micro-inverters have additional advantages: AC power is simpler to connect to a building's electrical system, they operate at safer voltages than central inverters (200–300 V, as opposed to 600 or 1000 V), and inverter failure means the loss of only a single module, not an entire array. However micro-inverters are not yet as reliable as large inverters, especially at high temperatures.

With these characteristics, MPP of individual modules is most suited to PV systems subject to shading or infrequent cleaning, and where the value of produced electricity is high. DC–DC and DC–AC module controllers are widely available in the market, and some modules now have DC–DC controllers built into them. They are used in both residential and commercial PV systems.

In PV systems designed to charge batteries for off-grid power systems, MPPT charge controllers are desirable to make the best use of all the energy generated by the panels. MPPT charge controllers are quickly becoming more affordable and more common. The benefits of MPPT regulators are greatest during cold weather, on cloudy or hazy days, or when the battery is deeply discharged. Peak-power trackers can be purchased separately or specified as an option with battery charge controllers or inverters. In all cases, however, the cost and complexity of adding a peak-power tracker should be balanced against the expected power gain and the impact on system reliability.

9.4 Applications

PV modules are designed for outdoor use under harsh conditions, such as marine, tropic, arctic, and desert environments. The PV array consists of a number of individual photovoltaic modules connected together to give a suitable current and voltage output. Common power modules have a rated power output of around 50–180 W each. As an example, a small system of 1.5–2 kWp may therefore comprise some 10–30 modules covering an area of around 15–25 m^2, depending on the technology used and the orientation of the array with respect to the sun.

Most power modules deliver direct current electricity at 12 V, whereas most common household appliances and industrial processes operate with alternating current at 240 or 415 V (120 V in the United States). Therefore, an inverter is used to convert the low-voltage DC to higher-voltage AC.

Other components in a typical PV system are the array mounting structure and various cables and switches needed to ensure that the PV generator can be isolated.

The basic principle of a PV system is shown in Figure 9.15. As can be seen, the PV array produces electricity, which can be directed from the controller to either battery storage or a load. Whenever there is no sunshine, the battery can supply power to the load if it has a satisfactory capacity.

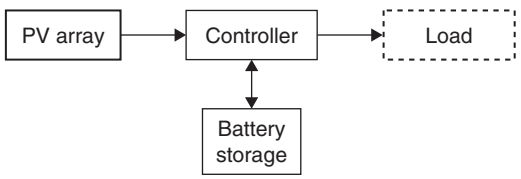

FIGURE 9.15

Basic principle of a PV solar energy system.

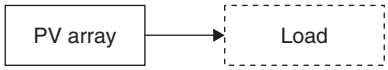

FIGURE 9.16

Schematic diagram of a direct-coupled PV system.

9.4.1 Direct-coupled PV system

In a direct-coupled PV system, the PV array is connected directly to the load. Therefore, the load can operate only whenever there is solar radiation, so such a system has very limited applications. The schematic diagram of such a system is shown in Figure 9.16. A typical application of this type of system is for water pumping, i.e., the system operates as long as sunshine is available, and instead of storing electrical energy, water is usually stored.

9.4.2 Stand-alone applications

Stand-alone PV systems are used in areas that are not easily accessible or have no access to an electric grid. A stand-alone system is independent of the electricity grid, with the energy produced normally being stored in batteries. A typical stand-alone system would consist of a PV module or modules, batteries, and a charge controller. An inverter may also be included in the system to convert the direct current generated by the PV modules to the alternating current form required by normal appliances. A schematic diagram of a stand-alone system is shown in Figure 9.17. As can be seen, the system can satisfy both DC and AC loads simultaneously.

9.4.3 Grid-connected system

Nowadays, it is usual practice to connect PV systems to the local electricity network. This means that, during the day, the electricity generated by the PV system can either be used immediately (which is normal for systems installed in offices, other commercial buildings, and industrial applications) or be sold to one of the electricity supply companies (which is more common for domestic systems, where the occupier may be out during the day). In the evening, when the solar system is unable to provide the

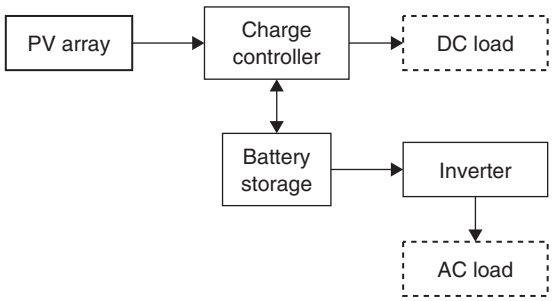

FIGURE 9.17

Schematic diagram of a stand-alone PV application.

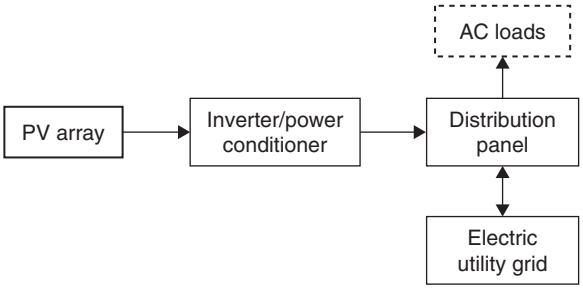

FIGURE 9.18

Schematic diagram of a grid-connected system.

electricity required, power can be bought back from the network. In effect, the grid is acting as an energy storage system, which means the PV system does not need to include battery storage. A schematic diagram of a grid-connected system is shown in Figure 9.18.

9.4.4 Hybrid-connected system

In the hybrid-connected system, more than one type of electricity generator is employed. The second type of electricity generator can be renewable, such as a wind turbine, or conventional, such as a diesel engine generator or the utility grid. The diesel engine generator can also be a renewable source of electricity when the diesel engine is fed with biofuels. A schematic diagram of a hybrid-connected system is shown in Figure 9.19. Again, in this system, both DC and AC loads can be satisfied simultaneously.

9.4.5 Types of applications

These are some of the most common PV applications:

- *Remote-site electrification.* Photovoltaic systems can provide long-term power at sites far from utility grids. The loads include lighting, small appliances, water pumps (including small

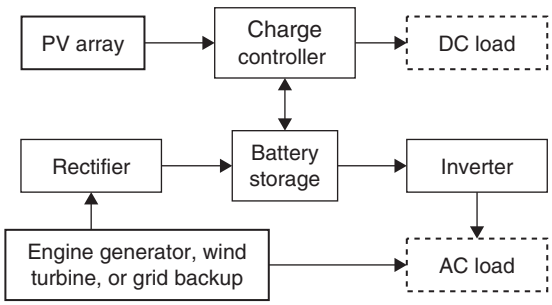

FIGURE 9.19

Schematic diagram of a hybrid connected system.

circulators of solar water heating systems), and communications equipment. In these applications, the load demand can vary from a few watts to tens of kilowatts. Usually, PV systems are preferred to fuel generators, since they do not depend on a fuel supply, which can be problematic, and they do avoid maintenance and environmental pollution problems.

- *Communications.* Photovoltaics can provide reliable power for communication systems, especially in remote locations, away from the utility grid. Examples include communication relay towers, travelers' information transmitters, cellular telephone transmitters, radio relay stations, emergency call units, and military communication facilities. Such systems range in size from a few watts for callbox systems to several kilowatts for relay stations. Obviously, these systems are stand-alone units in which PV-charged batteries provide a stable DC voltage that meets the varying current demand. Practice has shown that such PV power systems can operate reliably for a long time with little maintenance.
- *Remote monitoring.* Because of their simplicity, reliability, and capacity for unattended operation, photovoltaic modules are preferred in providing power at remote sites to sensors, data loggers, and associated meteorological monitoring transmitters, irrigation control, and monitoring highway traffic. Most of these applications require less than 150 W and can be powered by a single photovoltaic module. The batteries required are often located in the same weather-resistant enclosure as the data acquisition or monitoring equipment. Vandalism may be a problem in some cases; however, mounting the modules on a tall pole may solve the problem and avoid damage from other causes.
- *Water pumping.* Stand-alone photovoltaic systems can meet the need for small to intermediate-size water-pumping applications. These include irrigation, domestic use, village water supply, and livestock watering. Advantages of using water pumps powered by photovoltaic systems include low maintenance, ease of installation, and reliability. Most pumping systems do not use batteries but store the pumped water in holding tanks.
- *Charging vehicle batteries.* When not in use, vehicle batteries self-discharge over time. This is a problem for organizations that maintain a fleet of vehicles, such as the fire-fighting services. Photovoltaics battery chargers can help solve this problem by keeping the battery at a high state of charge by providing a trickle charging current. In this application, the modules can be installed on the roof of a building or car park (also providing shading) or on the vehicle itself. Another important application in this area is the use of PV modules to charge the batteries of electric vehicles.
- *Building-integrated photovoltaics.* BIPVs is a special application in which PVs are installed either in the façade or roof of a building and are an integral part of the building structure, replacing in each case the particular building component. To avoid an increase in the thermal load of the building, usually a gap is created between the PV and the building element (brick, slab, etc.), which is behind the PV, and in this gap, ambient air is circulated so as to remove the produced heat. During wintertime, this air is directed into the building to cover part of the building load; during summer, it is just rejected back to ambient at a higher temperature. A common example where these systems are installed is what is called *zero-energy houses*, where the building is an energy-producing unit that satisfies all its own energy needs. In another application related to buildings, PVs can be used as effective shading devices.
  As this is an important application it is examined in more detail in the following section.

Building-integrated photovoltaics

According to Sick and Erge (1996), approximately 25–30% of energy consumed in buildings in industrialized countries is electricity. Photovoltaics can be integrated on virtually every structure. Grid-connected BIPV is the simplest low-voltage residential system which comprises a PV array and inverter. They feed electricity directly to an electricity grid and do not usually require batteries. The performance of a BIPV grid-connected system depends on PV efficiency, local climate, the orientation and inclination of the PV array, load characteristics and the inverter performance. A comprehensive review on BIPV systems is presented by Norton et al. (2011).

BIPV displaces conventional building materials, which leads to savings in the purchase and installation of conventional materials, thus the net cost of the BIPV is lower, which increases the cost effectiveness of the system. There would be some additional cost associated with the BIPV wiring, but this would be minimal in a new construction. BIPV walls, roofs, and sunshades provide fully integrated electricity generation while also serving as part of the weather protective building envelope (Archer and Hill, 2001). BIPV can serve as a shading device for a window, a semi-transparent glass facade, a building exterior cladding panel, a skylight, parapet unit or roofing system.

The sizing and design of a BIPV system is based on a building's electrical load profile, PV output and balance-of-system characteristics, but must also consider building design constraints and its location, the local climate, and possible future increase of the load. A realistic estimation of load profile to be satisfied is the first step in the design of a stand-alone BIPV system design. In grid-connected BIPV applications the economically optimal diurnal load that must be met by the PV may not correspond to the total load, particularly at night and during wintertime.

There are also regulatory requirements concerning buildings that must be met; most local building codes and product certification requirements will specify specific standards for BIPV mounting, fixing, and fire resistance. These will often vary with the location of the building to take account of possible differences in wind loading, earthquake risk, and the attendant risks associated with particular failure modes (Norton et al., 2011). For this purpose, a product certification is required, usually carried out in an independent testing laboratory after passing satisfactorily a prescribed set of testing procedures (e.g. cycling of humidity, freeze/thaw, temperature, rain).

An advantage of BIPV is that as some of the PV power could be used in the building, the demand on the power grid is reduced and the reliability of supplied power to the building is improved. Another potential significant advantage is that the heat collected by PV modules can also be used for space heating or hot water-heating (see Section 9.8).

From architectural, technical and financial perspectives, building-integrated photovoltaics:

- Reduce the initial investment costs by displacing facade/roof/shading elements.
- Are aesthetically appealing.
- Electricity is generated at the point of use, reducing the costs and losses associated with transmission and distribution.
- Are suitable for installation on roofs and facades in densely populated areas.
- Require no additional land area for the installation.
- Can satisfy all, or a considerable part, of the electricity consumption of the building.
- Can act as a shading device.
- Can act as a source of day lighting if semi-transparent PVs are used for fenestration.
- Can provide part of the hot water or space-heating loads of the building.

Roofs are an attractive location for BIPV (Norton et al., 2011):

- They offer unshaded solar access.
- Cost is partially offset by the displacement of roofing materials by BIPV modules.
- Flat roofs generally enable more optimal solar cell placement and orientation.
- In a pitched roof which is near optimally inclined, the need for and cost of a support frame is eliminated.

Fully integrated BIPV roofing systems must perform the function of a standard roof and provide water tightness, drainage, and insulation.

PV glass curtain-walls and PV metal curtain-walls are used for integration of PV modules with wall materials (Toyokawa and Uehara, 1997). BIPV can be integrated into the building facade as:

- Rainscreen overcladding.
- Structural glazing mullion/transom curtain-wall systems.
- Panel curtain-wall systems.
- Profile metal cladding.

The performance ratio (PR) expresses the performance of a PV system in comparison to a system with no losses of the same design and rating at the same location. It is equal to the system efficiency under realistic reporting conditions (RRCs) divided by the module efficiency under standard test conditions (STCs) (Simmons and Infield, 1996). It indicates how close a PV system approaches ideal performance during real operation (Blaesser, 1997). The PR is independent of location and is influenced by:

- Insolation (remember that the efficiency of PV array depends on irradiance).
- The efficiency of the various system components.
- Size of the inverter relative to the PV array.
- Utilization factor of the system (i.e., the extent to which the system output is used).

9.5 Design of PV systems

The electrical power output from a PV panel depends on the incident radiation, the cell temperature, the solar incidence angle, and the load resistance. In this section, a method to design a PV system is presented and all these parameters are analyzed. Initially, a method to estimate the electrical load of an application is presented, followed by the estimation of the absorbed solar radiation from a PV panel and a description of the method for sizing PV systems.

9.5.1 Electrical loads

As is already indicated, a PV system size may vary from a few watts to hundreds of kilowatts. In grid-connected systems, the installed power is not so important because the produced power, if not consumed, is fed into the grid. In stand-alone systems, however, the only source of electrical power is the PV system; therefore, it is very important at the initial stages of the system design to assess the electrical loads the system will cover. This is especially important in emergency

warning systems. The main considerations that a PV system designer needs to address from the very beginning are:

1. According to the type of loads that the PV system will meet, which is more important, the total daily energy output or the average or peak power?
2. At what voltage will the power be delivered, and is it AC or DC?
3. Is a backup energy source needed?

Usually the first things the designer has to estimate are the load and the load profile that the PV system will meet. It is very important to be able to estimate precisely the loads and their profiles (time when each load occurs). Due to the initial expenditure needed, the system is sized at the minimum required to satisfy the specific demand. If, for example, three appliances exist, requiring 500 W, 1000 W, and 1500 W, respectively; each appliance is to operate for 1 h; and only one appliance is on at a time, then the PV system must have an installed peak power of 1500 W and 3000 Wh of energy requirement. If possible, when using a PV system, the loads should be intentionally spread over a period of time to keep the system small and thus cost-effective. Generally, the peak power is estimated by the value of the highest power occurring at any particular time, whereas the energy requirement is obtained by multiplying the wattage of each appliance by the operating hours and summing the energy requirements of all appliances connected to the PV system. The maximum power can easily be estimated with the use of a time-schedule diagram, as shown in the following example.

EXAMPLE 9.4

Estimate the daily load and the peak power required by a PV system that has three appliances connected to it with the following characteristics:

1. Appliance 1, 20 W operated for 3 h (10 am−1 pm).
2. Appliance 2, 10 W operated for 8 h (9 am−5 pm).
3. Appliance 3, 30 W operated for 2 h (2 pm−4 pm).

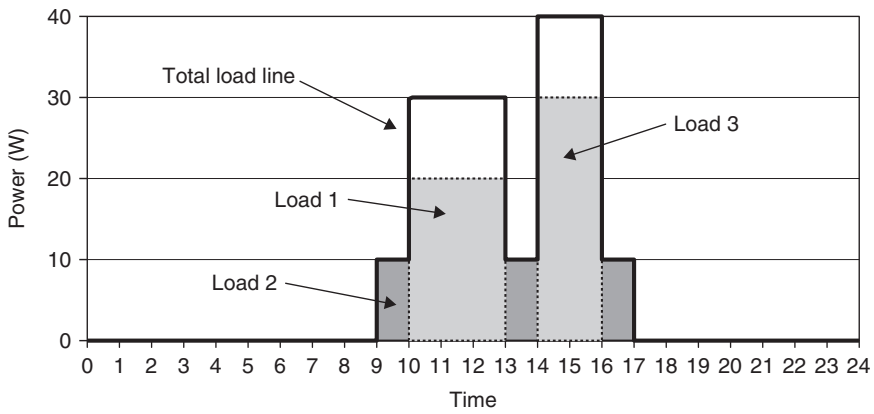

FIGURE 9.20

Time schedule diagram.

Solution

The daily energy use is equal to:

$$(20\ \text{W}) \times (3\ \text{h}) + (10\ \text{W}) \times (8\ \text{h}) + (30\ \text{W}) \times (2\ \text{h}) = 200\ \text{Wh}$$

To find the peak power, a time schedule diagram is required (see Figure 9.20). As can be seen, the peak power is equal to 40 W.

EXAMPLE 9.5

A remote cottage has the loads listed in Table 9.2. Find the average load and peak power to be satisfied by a 12 V PV system with an inverter.

Table 9.2 Loads for Cottage in Example 9.5

Appliance Type	Description	Power Type	Period of Operation
Lights	3, 25 W compact fluorescent bulbs, daily	DC	Nighttime 5 h each
Light	11 W compact fluorescent bulb, daily	AC	Nighttime 5 h
Water pump	50 W (6 A start current), daily	DC	Daytime 2 h
Oven	500 W, 3 times a week	AC	Daytime 1.5 h
Steam iron	800 W, once a week	AC	Daytime 1.5 h

Solution

In Table 9.3, the loads for this application are separated according to type of power. Because no information is given about the time schedule of the loads, these are assumed to occur simultaneously.

Table 9.3 Loads in Table 9.2, by Type of Power

Appliance Type	Power Type	Power (W)	Run Time (h)	Energy/Day (Wh)	Energy/Week (Wh)
Lights	DC	$3 \times 25 = 75$ W	5	375	2625
Lights	AC	11 W	5	55	385
Water pump	DC	50 W	2	100	700
Oven	AC	500 W	1.5	–	2250
Steam iron	AC	800 W	1.5	–	1200

From Table 9.3, the following can be determined:

$$\text{Average DC load} = 375 + 100 = 475 \text{ Wh/day}$$

$$\text{Average AC load} = (385 + 2250 + 1200)/7 = 547.9 \text{ Wh/day}$$

$$\text{Peak DC load} = 6 \times 12 + 75 = 147 \text{ W (the maximum occurs when the pump starts, } 6 \times 12 > 50 \text{ W)}$$

$$\text{Peak AC load} = 11 + 500 + 800 = 1311 \text{ W}$$

9.5.2 Absorbed solar radiation

The main factor affecting the power output from a PV system is the absorbed solar radiation, S, on the PV surface. As was seen in Chapter 3, S depends on the incident radiation, air mass, and incident angle. As in the case of thermal collectors, when radiation data on the plane of the PV are unknown, it is necessary to estimate the absorbed solar radiation using the horizontal data and information on incidence angle. As in thermal collectors, the absorbed solar radiation includes the beam, diffuse, and ground-reflected components. In the case of PVs, however, a spectral effect is also included. Therefore, by assuming that the diffuse and ground-reflected radiation is isotropic, S can be obtained from (Duffie and Beckman, 2006):

$$S = M\left\{G_B R_B(\tau\alpha)_B + G_D(\tau\alpha)_D\left[\frac{1+\cos(\beta)}{2}\right] + G\rho_G(\tau\alpha)_G\left[\frac{1-\cos(\beta)}{2}\right]\right\} \tag{9.25}$$

where M = air mass modifier.

The air mass modifier, M, accounts for the absorption of radiation by species in the atmosphere, which causes the spectral content of the available solar radiation to change, thus altering the spectral distribution of the incident radiation and the generated electricity. An empirical relation that accounts for the changes in the spectral distribution resulting from changes in the air mass, m, from the reference air mass of 1.5 (at sea level) is given by the following empirical relation developed by King et al. (2004):

$$M = \alpha_0 + \alpha_1 m + \alpha_2 m^2 + \alpha_3 m^3 + \alpha_4 m^4 \tag{9.26}$$

Constant α_i values in Eq. (9.26) depend on the PV material, although for small zenith angles, less than about 70°, the differences are small (De Soto et al., 2006). Table 9.4 gives the values of the α_i constants for various PV panels tested at the National Institute of Standards and Technology (NIST) (Fanney et al., 2002).

As was seen in Chapter 2, Section 2.3.6, the air mass, m, is the ratio of the mass of air that the beam radiation has to traverse at any given time and location to the mass of air that the beam radiation would traverse if the sun were directly overhead. This can be given from Eq. (2.81) or from the following relation developed by King et al. (1998):

$$m = \frac{1}{\cos(\Phi) + 0.5050(96.08 - \Phi)^{-1.634}} \tag{9.27}$$

Table 9.4 Values of α_i Constants for Various PV Panels Tested at NIST

Cell Type	Silicon Thin Film	Monocrystalline	Polycrystalline	Three-Junction Amorphous
α_0	0.938110	0.935823	0.918093	1.10044085
α_1	0.062191	0.054289	0.086257	−0.06142323
α_2	−0.015021	−0.008677	−0.024459	−0.00442732
α_3	0.001217	0.000527	0.002816	0.000631504
α_4	−0.000034	−0.000011	−0.000126	-1.9184×10^{-5}

As the incidence angle increases, the amount of radiation reflected from the PV cover increases. Significant effects of inclination occur at incidence angles greater than 65°. The effect of reflection and absorption as a function of incidence angle is expressed in terms of the incidence angle modifier, K_θ, defined as the ratio of the radiation absorbed by the cell at incidence angle θ divided by the radiation absorbed by the cell at normal incidence. Therefore, in equation form, the incidence angle modifier at angle θ is obtained by:

$$K_\theta = \frac{(\tau\alpha)_\theta}{(\tau\alpha)_n} \tag{9.28}$$

It should be noted that the incidence angle depends on the PV panel slope, location, and time of the day. As in thermal collectors, separate incidence angle modifiers are required for the beam, diffuse, and ground-reflected radiation. For the diffuse and ground-reflected radiation, the effective incidence angle given by Eq. (3.4) can be used. Although these equations were obtained for thermal collectors, they were found to give reasonable results for PV systems as well.

So, using the concept of incidence angle modifier and noting that:

$$K_{\theta,\mathrm{B}} = \frac{(\tau\alpha)_\mathrm{B}}{(\tau\alpha)_n}, K_{\theta,\mathrm{D}} = \frac{(\tau\alpha)_\mathrm{D}}{(\tau\alpha)_n}, K_{\theta,\mathrm{G}} = \frac{(\tau\alpha)_\mathrm{G}}{(\tau\alpha)_n}$$

Equation (9.25) can be written as:

$$S = (\tau\alpha)_n M\left\{G_\mathrm{B}R_\mathrm{B}K_{\theta,\mathrm{B}} + G_\mathrm{D}K_{\theta,\mathrm{D}}\left[\frac{1+\cos(\beta)}{2}\right] + G\rho_\mathrm{G}K_{\theta,\mathrm{G}}\left[\frac{1-\cos(\beta)}{2}\right]\right\} \tag{9.29}$$

It should be noted that, because the glazing is bonded to the cell surface, the incidence angle modifier of a PV panel differs slightly from that of a flat-plate collector and is obtained by combining the various equations presented in Chapter 2, Section 2.3.3:

$$(\tau\alpha)_\theta = e^{-[KL/\cos(\theta_\mathrm{r})]}\left\{1 - \frac{1}{2}\left[\frac{\sin^2(\theta_\mathrm{r}-\theta)}{\sin^2(\theta_\mathrm{r}+\theta)} + \frac{\tan^2(\theta_\mathrm{r}-\theta)}{\tan^2(\theta_\mathrm{r}+\theta)}\right]\right\} \tag{9.30}$$

where θ and θ_r are the incidence angle and refraction angle (same as angles θ_1 and θ_2 in Section 2.3.3). A typical value of the extinction coefficient, K, for PV systems is $4\mathrm{m}^{-1}$ (for water white glass), glazing thickness is 2 mm, and the refractive index for glass is 1.526.

Table 9.5 Values of b_i Constants for Various PV Panels Tested at NIST

Cell Type	Silicon Thin Film	Monocrystalline	Polycrystalline	Three-Junction Amorphous
b_0	0.998980	1.000341	0.998515	1.001845
b_1	−0.006098	−0.005557	−0.012122	−0.005648
b_2	8.117×10^{-4}	6.553×10^{-4}	1.440×10^{-3}	7.250×10^{-4}
b_3	-3.376×10^{-5}	-2.733×10^{-5}	-5.576×10^{-5}	-2.916×10^{-5}
b_4	5.647×10^{-7}	4.641×10^{-7}	8.779×10^{-7}	4.696×10^{-7}
b_5	-3.371×10^{-9}	-2.806×10^{-9}	-4.919×10^{-9}	-2.739×10^{-9}

A simpler way to obtain the incidence angle modifier is given by King et al. (1998), who suggested the following equation:

$$K_\theta = b_0 + b_1\theta + b_2\theta^2 + b_3\theta^3 + b_4\theta^4 + b_5\theta^5 \tag{9.31}$$

Table 9.5 gives the values of the b_i constants for various PV panels tested at NIST (Fanney et al., 2002).

Therefore, Eq. (9.31) can be used directly for the specific type of cell to give the incidence angle modifier according to the incidence angle. Again, for the diffuse and ground-reflected radiation, the effective incidence angle given by Eq. (3.4) can be used.

EXAMPLE 9.6

A south-facing PV panel is installed at 30° in a location which is at 35°N latitude. If, on June 11 at noon, the beam radiation is 715 W/m^2 and the diffuse radiation is 295 W/m^2, both on a horizontal surface, estimate the absorbed solar radiation on the PV panel. The thickness of the glass cover on PV is 2 mm, the extinction coefficient K is 4m^{-1}, and ground reflectance is 0.2.

Solution

From Table 2.1, on June 11, $\delta = 23.09°$. First, the effective incidence angles need to be calculated. For the beam radiation, the incidence angle is required, estimated from Eq. (2.20):

$$\cos(\theta) = \sin(L-\beta)\sin(\delta) + \cos(L-\beta)\cos(\delta)\cos(h)$$
$$= \sin(35-30)\sin(23.09) + \cos(35-30)\cos(23.09)\cos(0) = 0.951 \text{ or } \theta = 18.1°$$

For the diffuse and ground-reflected components, Eq. (3.4) can be used:

$$\theta_{e,D} = 59.68 - 0.1388\beta + 0.001497\beta^2 = 59.68 - 0.1388(30) + 0.001497(30)^2 = 56.9°$$

$$\theta_{e,G} = 90 - 0.5788\beta + 0.002693\beta^2 = 90 - 0.5788(30) + 0.002693(30)^2 = 75.1°$$

Next, we need to estimate the three incidence angle modifiers. At an incidence angle of 18.1°, the refraction angle from Eq. (2.44) is:

$$\sin(\theta_r) = \sin(\theta)/1.526 = \sin(18.1)/1.526 = 0.204 \text{ or } \theta_r = 11.75^\circ$$

Using Eq. (9.30) with $K = 4\text{m}^{-1}$ and $L = 0.002$ m,

$$(\tau\alpha)_B = e^{-[KL/\cos(\theta_r)]}\left\{1 - \frac{1}{2}\left[\frac{\sin^2(\theta_r - \theta)}{\sin^2(\theta_r + \theta)} + \frac{\tan^2(\theta_r - \theta)}{\tan^2(\theta_r + \theta)}\right]\right\}$$

$$= e^{-[0.008/\cos(11.75)]}\left\{1 - \frac{1}{2}\left[\frac{\sin^2(11.75 - 18.1)}{\sin^2(11.75 + 18.1)} + \frac{\tan^2(11.75 - 18.1)}{\tan^2(11.75 + 18.1)}\right]\right\} = 0.9487$$

At normal incidence, as shown in Chapter 2, Section 2.3.3, Eq. (2.49), the term in the square bracket of Eq. (9.30) is replaced with $1 - [(n-1)/(n+1)]^2$. Therefore,

$$(\tau\alpha)_n = \text{e}^{-KL}\left[1 - \left(\frac{n-1}{n+1}\right)^2\right] = \text{e}^{-0.008}\left[1 - \left(\frac{1.526 - 1}{1.526 + 1}\right)^2\right] = 0.9490$$

And from Eq. (9.28),

$$K_{\theta,B} = \frac{(\tau\alpha)_B}{(\tau\alpha)_n} = \frac{0.9487}{0.9490} = 0.9997$$

For the diffuse radiation,

$$\sin(\theta_r) = \sin(\theta_{e,D})/1.526 = \sin(56.9)/1.526 = 0.5490 \text{ or } \theta_r = 33.3^\circ$$

Using Eq. (9.30),

$$(\tau\alpha)_D = \text{e}^{-[KL/\cos(\theta_r)]}\left\{1 - \frac{1}{2}\left[\frac{\sin^2(\theta_r - \theta_{e,D})}{\sin^2(\theta_r + \theta_{e,D})} + \frac{\tan^2(\theta_r - \theta_{e,D})}{\tan^2(\theta_r + \theta_{e,D})}\right]\right\}$$

$$= \text{e}^{-[0.008/\cos(33.3)]}\left\{1 - \frac{1}{2}\left[\frac{\sin^2(33.3 - 56.9)}{\sin^2(33.3 + 56.9)} + \frac{\tan^2(33.3 - 56.9)}{\tan^2(33.3 + 56.9)}\right]\right\} = 0.9111$$

And from Eq. (9.28),

$$K_{\theta,D} = \frac{(\tau\alpha)_D}{(\tau\alpha)_n} = \frac{0.9111}{0.9490} = 0.9601$$

Using Eq. (9.31) for monocrystalline cells gives $K_{\theta,D} = 0.9622$; and for polycrystalline cells, $K_{\theta,D} = 0.9672$. Both values are close to the value just obtained, so even if the exact type of PV cell is not known, acceptable values can be obtained from Eq. (9.31) using either type of the cell.

For the ground-reflected radiation,

$$\sin(\theta_r) = \sin(\theta_{e,G})/1.526 = \sin(75.1)/1.526 = 0.6333 \text{ or } \theta_r = 39.29^\circ$$

Using Eq. (9.30),

$$(\tau\alpha)_{\mathrm{G}} = \mathrm{e}^{-[KL/\cos(\theta_r)]}\left\{1-\frac{1}{2}\left[\frac{\sin^2(\theta_{\mathrm{r}}-\theta_{\mathrm{e,G}})}{\sin^2(\theta_{\mathrm{r}}+\theta_{\mathrm{e,G}})}+\frac{\tan^2(\theta_{\mathrm{r}}-\theta_{\mathrm{e,G}})}{\tan^2(\theta_{\mathrm{r}}+\theta_{\mathrm{e,G}})}\right]\right\}$$

$$= \mathrm{e}^{-[0.008/\cos(39.29)]}\left\{1-\frac{1}{2}\left[\frac{\sin^2(39.29-75.1)}{\sin^2(39.29+75.1)}+\frac{\tan^2(39.29-75.1)}{\tan^2(39.29+75.1)}\right]\right\} = 0.7325$$

And from Eq. (9.28),

$$K_{\theta,\mathrm{G}} = \frac{(\tau\alpha)_{\mathrm{G}}}{(\tau\alpha)_n} = \frac{0.7325}{0.9490} = 0.7719$$

Using Eq. (9.31) for monocrystalline cells gives $K_{\theta,\mathrm{G}} = 0.7625$, and for polycrystalline cells, $K_{\theta,\mathrm{G}} = 0.7665$. Both values, again, are close to the value obtained previously.

For the estimation of the air mass, the zenith angle is required, obtained from Eq. (2.12):

$$\cos(\Phi) = \sin(L)\sin(\delta)+\cos(L)\cos(\delta)\cos(h)$$

$$= \sin(35)\sin(23.09)+\cos(35)\cos(23.09)\cos(0) = 0.9785 \text{ or } \Phi = 11.91^\circ$$

The air mass is obtained from Eq. (9.27):

$$m = \frac{1}{\cos(\Phi)+0.5050(96.08-\Phi)^{-1.634}}$$

$$= \frac{1}{\cos(11.91)+0.5050(96.08-11.91)^{-1.634}} = 1.022$$

It should be noted that the same result is obtained using Eq. (2.81):

$$m = \frac{1}{\cos(\Phi)} = 1.022$$

From Eq. (9.26),

$$M = \alpha_0+\alpha_1 m+\alpha_2 m^2+\alpha_3 m^3+\alpha_4 m^4$$

$$= 0.935823+0.054289\times(1.022)-0.008677\times(1.022)^2+0.000527\times(1.022)^3$$

$$-0.000011\times(1.022)^4 = 0.9828$$

From Eq. (2.88),

$$R_{\mathrm{B}} = \frac{\cos(\theta)}{\cos(\Phi)} = \frac{\cos(18.1)}{\cos(11.91)} = 0.971$$

Now, using Eq. (9.29),

$$S = (\tau\alpha)_n M\left\{G_B R_B K_{\theta,B} + G_D K_{\theta,D}\left[\frac{1+\cos(\beta)}{2}\right] + G\rho_G K_{\theta,G}\left[\frac{1-\cos(\beta)}{2}\right]\right\}$$

$$= 0.9490 \times 0.9828\left\{715 \times 0.971 \times 0.9997 + 295 \times 0.9601\left[\frac{1+\cos(30)}{2}\right] + 1010 \times 0.2 \times 0.7719\left[\frac{1-\cos(30)}{2}\right]\right\} = 903.5 \text{ W/m}^2$$

9.5.3 Cell temperature

As was seen in Section 9.1.3, the performance of the solar cell depends on the cell temperature. This temperature can be determined by an energy balance and considering that the absorbed solar energy that is not converted to electricity is converted to heat, which is dissipated to the environment. Generally, when operating solar cells at elevated temperatures, their efficiency is lowered. In cases where this heat dissipation is not possible, as in BIPVs and concentrating PV systems (see Section 9.7), the heat must be removed by some mechanical means, such as forced air circulation, or by a water heat exchanger in contact with the back side of the PV. In this case, the heat can be used to an advantage, as explained in Section 9.8; these systems are called *hybrid photovoltaic/thermal* (PV/T) systems. Because these systems offer a number of advantages, even normal roof-mounted PVs can be converted into hybrid PV/Ts.

The energy balance on a unit area of a PV module that is cooled by heat dissipation to ambient air is given by:

$$(\tau\alpha)G_t = \eta_e G_t + U_L(T_C - T_a) \tag{9.32}$$

For the $(\tau\alpha)$ product, a value of 0.9 can be used without serious error (Duffie and Beckman, 2006). The heat loss coefficient, U_L, includes losses by convection and radiation from the front and back of the PV to the ambient temperature, T_a.

By operating the module at the nominal operating cell temperature (NOCT) conditions (see Table 9.1) with no load, i.e. $\eta_e = 0$, Eq. (9.32) becomes:

$$(\tau\alpha)G_{t,NOCT} = U_L(T_{NOCT} - T_{a,NOCT}) \tag{9.33}$$

which can be used to determine the ratio:

$$\frac{(\tau\alpha)}{U_L} = \frac{T_{NOCT} - T_{a,NOCT}}{G_{t,NOCT}} \tag{9.34}$$

By substituting Eq. (9.34) into Eq. (9.32) and performing the necessary manipulations, the following relation can be obtained:

$$T_C = (T_{NOCT} - T_{a,NOCT})\left[\frac{G_t}{G_{t,NOCT}}\right]\left[1 - \frac{\eta_e}{(\tau\alpha)}\right] + T_a \tag{9.35}$$

An empirical formula that can be used for the calculation of PV module temperature of polycrystalline silicon solar cells was presented by Lasnier and Ang (1990). This is a function of the ambient temperature, T_a, and the incoming solar radiation, G_t, given by:

$$T_C = 30 + 0.0175(G_t - 300) + 1.14(T_a - 25) \tag{9.36}$$

When the temperature coefficient of the PV module is given, the following equation can be used to estimate the efficiency according to the cell temperature:

$$\eta_e = \eta_R[1 - \beta(T_C - T_{NOCT})] \tag{9.37}$$

where

β = temperature coefficient (per k^{-1}).
η_R = reference efficiency.

EXAMPLE 9.7

If, for a PV module operating at NOCT conditions, the cell temperature is 42 °C, determine the cell temperature when this module operates at a location where $G_t = 683\ W/m^2$, $V = 1$ m/s, and $T_a = 41$ °C and the module is operating at its maximum power point with an efficiency of 9.5%.

Solution

Using Eq. (9.35),

$$T_C = (T_{NOCT} - T_{a,NOCT})\left[\frac{G_t}{G_{t,NOCT}}\right]\left[1 - \frac{\eta_e}{(\tau\alpha)}\right] + T_a$$

$$= (42 - 20)\left[\frac{683}{800}\right]\left(1 - \frac{0.095}{0.9}\right) + 41 = 57.8\ °C$$

Using empirical Eq. (9.36),

$$T_C = 30 + 0.0175(683 - 300) + 1.14(41 - 25) = 54.9\ °C$$

As can be seen, the empirical method is not as accurate but offers a good approximation.

It should be noted that, in Example 9.7, the module efficiency was given. If it was not given, then a trial-and-error solution needs to be applied. In this procedure, a value of module efficiency is assumed and T_C is estimated using Eq. (9.35). Provided that I_o and I_{sc} are known, the value of T_C is used to find V_{max} with Eq. (9.14). Subsequently, P_{max} and η_{max} are estimated with Eqs (9.17) and (9.18), respectively. The initial guess value of η_e is then compared with η_{max}, and if there is a difference, iteration is used. Because the efficiency is strongly related to cell temperature, fast convergence is achieved.

9.5.4 Sizing of PV systems

Once the load and absorbed solar radiation are known, the design of the PV system can be carried out, including the estimation of the required PV panel's area and the selection of the other equipment, such as controllers and inverters. Detailed simulations of PV systems can be carried with the TRNSYS

program (see Chapter 11, Section 11.5.1); however, usually a simple procedure needs to be followed to perform a preliminary sizing of the system. The simplicity of this preliminary design depends on the type of the application. For example, a situation in which a vaccine refrigerator is powered by the PV system, and a possible failure of the system to supply the required energy will destroy the vaccines is much different to a home system delivering electricity to a television and some lamps.

The energy delivered by a PV array, E_{PV}, is given by:

$$E_{PV} = A\eta_e\overline{G}_t \tag{9.38}$$

where

$\overline{G}_t$ = monthly average value of G_t, obtained from Eq. (2.97) by setting all parameters as monthly average values.
A = area of the PV array (m^2).

The energy of the array available to the load and battery, E_A, is obtained from Eq. (9.38) by accounting for the array losses, L_{PV}, and other power conditioning losses, L_C:

$$E_A = E_{PV}(1 - L_{PV})(1 - L_C) \tag{9.39}$$

Therefore, the array efficiency is defined as:

$$\eta_A = \frac{E_A}{A\overline{G}_t} \tag{9.40}$$

Grid-connected systems

The inverter size required for grid-connected systems is equal to the nominal array power. The energy available to the grid is simply what is produced by the array multiplied by the inverter efficiency:

$$E_{grid} = E_A\eta_{inv} \tag{9.41}$$

Usually, some distribution losses are present accounted by η_{dist} and, if not, all this energy can be absorbed by the grid, then the actual energy delivered, E_d, is obtained by accounting for the grid absorption rate, η_{abs}, from:

$$E_d = E_{grid}\eta_{abs}\eta_{dist} \tag{9.42}$$

Stand-alone systems

For stand-alone systems, the total equivalent DC demand, $D_{dc,eq}$, is obtained by summing the total DC demand, D_{dc}, and the total AC demand, D_{ac} (both expressed in kilowatt hours per day), converted to DC equivalent using:

$$D_{dc,eq} = D_{dc} + \frac{D_{ac}}{\eta_{inv}} \tag{9.43}$$

When the array supplies all energy to a DC load, the actual energy delivered, $E_{d,dc}$, is obtained by:

$$E_{d,dc} = E_A\eta_{dist} \tag{9.44}$$

When the battery directly supplies a DC load, the efficiency of the battery, η_{bat}, is accounted for, and the actual energy delivered, $E_{d,dc,bat}$, is obtained from:

$$E_{d,dc,bat} = E_A \eta_{bat} \eta_{dist} \tag{9.45}$$

When the battery is used to supply energy to an AC load, the inverter efficiency is also accounted for:

$$E_{d,ac,bat} = E_A \eta_{bat} \eta_{inv} \eta_{dist} \tag{9.46}$$

Finally, when the array supplies all energy to an AC load, the actual energy delivered, $E_{d,ac}$, is obtained by:

$$E_{d,ac} = E_A \eta_{inv} \eta_{dist} \tag{9.47}$$

This methodology is demonstrated by means of two examples. The first is a simple one and the second takes into account the various efficiencies.

EXAMPLE 9.8

A PV system is using 80 W, 12 V panels and 6 V, 155 Ah batteries in a good sunshine area. The battery efficiency is 73% and the depth of discharge is 70%. If, in wintertime, there are 5 h of daylight, estimate the number of PV panels and batteries required for a 24 V application with a load of 2600 Wh.

Solution

The number of PV panels required is obtained from:

$$\text{Number of panels} = 2600(\text{Wh/day})/[5(\text{h/day}) \times 80(\text{W/panel})] = 6.5, \text{round off to 7 panels}$$

Because the system voltage is 24 V and each panel produces 12 V, two panels need to be connected in series to produce the required voltage, so an even number is required; therefore, the number of PV panels is increased to eight.

If, for the location with good sunshine, we consider that three days of storage would be adequate, the storage required is:

$$2600(\text{Wh/day}) \times 3(\text{day})/(0.73 \times 0.7) = 15{,}264 \text{ Wh}$$

$$\text{Number of batteries required} = 15{,}264(\text{Wh})/[155(\text{Ah}) \times 6(\text{V})]$$

$$= 16.4, \text{rounded off to 17 batteries}$$

Again as the system voltage is 24 V and each battery is 6 V, we need to connect 4 batteries in series, so the number of batteries to use here is either 16 (very close to 16.4, with the possibility of not having enough power for the third day) or 20 (for more safety).

The second example uses the concept of efficiency of the various components of the PV system.

EXAMPLE 9.9

Using the data from Example 9.5, estimate the expected daily energy requirement. The efficiencies of the various components of the system are:

- Inverter = 90%.
- Battery = 75%.
- Distribution circuit = 95%.

Solution

From Example 9.5, the average DC load was 475 Wh and the average AC load was 547.9 Wh. These give a total load of 1022.9 Wh.

Expected daily loads are (from Example 9.5):

- Day DC = 100 Wh (from PV system).
- Night DC = 375 Wh (from battery).
- Night AC = 55 Wh (from battery).
- Day AC = 492.9 Wh, = (2250 + 1200)/7 (from PV system through the inverter).

The various energy requirements are obtained as follows:

- Day DC energy is obtained from Eq. (9.44): $E_{d,dc} = E_A \eta_{dist}$, so $E_A = 100/0.95 = 105.3$ Wh.
- Night DC energy is obtained from Eq. (9.45): $E_{d,dc,bat} = E_A \eta_{bat} \eta_{dist}$, so $E_A = 375/(0.75 \times 0.95) = 526.3$ Wh.
- Night AC energy is obtained from Eq. (9.46): $E_{d,ac,bat} = E_A \eta_{bat} \eta_{inv} \eta_{dist}$, so $E_A = 55/(0.75 \times 0.90 \times 0.95) = 85.8$ Wh.
- Day AC energy is obtained from Eq. (9.47): $E_{d,ac} = E_A \eta_{inv} \eta_{dist}$, so, $E_A = 492.9/(0.90 \times 0.95) = 576.5$ Wh.
- Expected daily energy requirement = 105.3 + 526.3 + 85.8 + 576.5 = 1293.9 Wh.

Therefore the energy requirement is increased by 27% compared to 1022.9 Wh estimated before.

One way utilities historically have thought about generation reliability is loss-of-load probability (LLP). LLP is the probability that a generation will be insufficient to meet demand at some point over some specific time window, and this principle can also be used in sizing stand-alone PV systems. Therefore, the merit of a stand-alone PV system should be judged in terms of the reliability of the electricity supply to the load. Specifically, for stand-alone PV systems, LLP is defined as the ratio between the energy deficit and the energy demands both on the load and over a long period of time. Because of the random nature of the solar radiation, the LLP of even a trouble-free PV system is always greater than 0.

Any PV system consists mainly of two subsystems that need to be designed: the PV array (also called the *generator*) and the battery storage system (also called the *accumulator*). A useful definition of these parameters relates to the load. Therefore, on a daily basis, the PV array capacity, C_A, is defined as the ratio between the mean PV array energy production and the mean load energy demand. The storage capacity, C_S, is defined as the maximum energy that can be taken out from the accumulator

divided by the mean load energy demand. According to Egido and Lorenzo (1992), the sizing pair C_A and C_S can be given by the following equations:

$$C_A = \frac{\eta_{PV} A H_t}{L} \tag{9.48}$$

$$C_S = \frac{C}{L} \tag{9.49}$$

where

A = PV array area (m^2).
η_{PV} = PV array efficiency.
H_t = mean daily irradiation on the PV array (Wh/m^2).
L = mean daily energy consumption (Wh).
C = useful accumulator capacity (Wh).

The reliability of a PV system is defined as the percentage of load satisfied by the PV system, whereas the LLP is the percentage of the mean load (over large periods of time) not supplied by the PV system, i.e., it is the opposite of reliability.

As can be understood from Eqs (9.48) and (9.49), it is possible to find many different combinations of C_A and C_S leading to the same LLP value. However, the larger the PV system size, the greater is the cost and the lower the LLP. Therefore, the task of sizing a PV system consists of finding the better trade-off between cost and reliability. Very often, the reliability is an *a priori* requirement from the user, and the problem is to find the pair of C_A and C_S values that lead to a given LLP value at the minimum cost.

Additionally, because C_A depends on the meteorological conditions of the location, this means that the same PV array for the same load can be "large" in one site and "small" in another site with lower solar radiation.

In cases where long-term averages of daily irradiation are available in terms of monthly means, Eq. (9.48) is modified as:

$$C'_A = \frac{\eta_{PV} A \overline{H}_t}{L} \tag{9.50}$$

where $\overline{H}_t$ = monthly average daily irradiation on the PV array (Wh/m^2).

In this case,C'_A is defined as the ratio of the average energy output of the generator in the month with worst solar radiation input divided by the average consumption of the load (assuming a constant consumption of load for every month).

Each point of the C_A–C_S plane represents a size of a PV system. This allows one to map the reliability, as is shown in Figure 9.21. The curve is the loci of all the points corresponding to a same LLP value. Because of that, this type of curve is called an *iso-reliability curve*. In Figure 9.21, an example LLP curve is represented for LLP equal to 0.01.

It should be noted that the definitions of C_A and C_S imply that this map is independent of the load and depends only on the meteorological behavior of the location. As can be seen from Figure 9.21, the iso-reliability curve is very nearly a hyperbola with its asymptotes parallel to the x and y axes, respectively. For a given LLP value, the plot of the cost of the PV systems (dashed line in Figure 9.21) corresponding to the iso-reliability curve is, approximately, a parabola having a minimum that defines the optimal solution to the sizing problem.

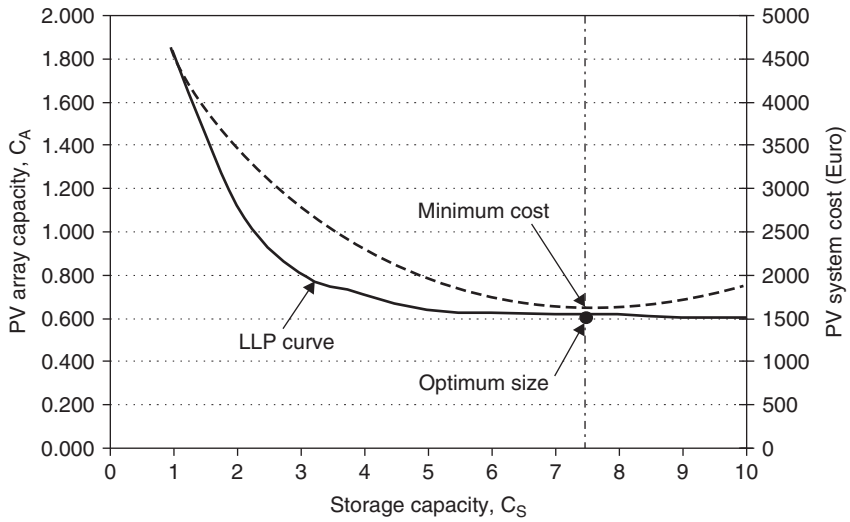

FIGURE 9.21

LLP curve for LLP = 0.01 and cost curve of a PV system.

The LLP curve represents pairs of C_S and C_A values that lead to the same value of LLP. This means, for example, that for the pair $(C_S, C_A) = (2, 1.1)$, the proposed reliability is achieved by having a "big" generator and a "small" storage system. Similarly, for the same reliability, the pair $(C_S, C_A) = (9, 0.6)$ leads to a "small" generator and a "big" battery. As can be seen, the optimum size of the system is at $(C_S, C_A) = (7.5, 0.62)$, which gives the minimum PV system cost.

Many methods have been developed by researchers to establish relations between C_A, C_S, and LLP. The main ones are numerical methods that use detailed system simulations and analytical methods that use equations describing the behavior of the PV system. These methods are presented by Egido and Lorenzo (1992).

Fragaki and Markvart (2008) developed a new sizing approach applied to stand-alone PV systems design, based on system configurations without shedding load. The investigation is based on a detailed study of the minimum storage requirement and an analysis of the sizing curves. The analysis revealed the importance of using daily series of measured solar radiation data instead of monthly average values. Markvart et al. (2006) presented the system sizing curve as superposition of contributions from individual climatic cycles of low daily solar radiation for a location southeast of England.

Hontoria et al. (2005) used an artificial neural network (ANN) (see Chapter 11) to generate the sizing curve of stand-alone PV systems from C_S, LLP, and daily clearness index. Mellit et al. (2005) also used an ANN architecture for estimating the sizing coefficients of stand-alone PV systems based on the synthetic and measured solar radiation data.

Once the LLP curves are obtained, it is very simple to design both the capacity of the generator (C_A) and the accumulator capacity (C_S). Depending on the reliability needed for the PV system design, a specific value of the LLP is considered. For instance, Table 9.6 shows some usual values for typical PV systems.

Table 9.6 Recommended LLP Values for Various Applications

Application	LLP
Domestic appliances	10^{-1}
Rural home lighting	10^{-2}
Telecommunications	10^{-4}

9.6 Tilt and yield

Photovoltaic modules are usually characterized by their peak-power output, kWp, measured under Standard Test Condition (also known as Standard Rating Condition, SRC). Another useful measure is the cumulative energy that a module generates over a period of time, as in practice electricity is bought and sold in kWh. Achieving the highest energy output, or "yield", at the lowest cost is often a primary goal of the solar engineer.

The yield of a PV module is proportional to the amount of solar irradiation it receives, which can be increased by using various modes of tilting and tracking as described in Section 2.2.1. When multiple modules are used, however, tilting them can cause shading between the different rows. Therefore it is useful to examine the relationship between energy yield, tilting, and module spacing.

It should be noted that a module's conversion efficiency, and thus yield, is influenced by conditions specific to local climate such as temperature, light intensity and spectrum. Also, different types of PV vary in their response to these factors. Therefore it is difficult to accurately predict a module's yield at a given location—even if irradiation levels there are well known (Huld et al., 2010).

9.6.1 Fixed tilt

The simplest method for increasing the solar flux received by a PV module is to mount it on a fixed frame that is tilted relative to the horizontal. There are two angles to consider: the collector tilt angle, β (deviation from the horizontal plane) and the collector azimuth angle, Z_s (deviation from due south, in the northern hemisphere).

Tilting the module at an angle equal to the local geographic latitude, a practice known as latitude tilt, minimizes the average incidence angle throughout the year. In practice a smaller tilt angle is often used in order to reduce shading of adjacent modules, minimize wind load, and take greater advantage of summer months when there is more solar flux and the sun is higher in the sky.

Considering only the goal of maximizing annual electricity yield, the tilt angle (β) would be modified from latitude angle (L) to collect more of summer's higher irradiation. It has been empirically determined that the optimal tilt angle for annual yield can be approximated by (Chang, 2009):

$$\beta = 0.764L + 2.14^\circ, \quad \text{for } L \leq 65^\circ \tag{9.51a}$$

$$\beta = 0.224L + 33.65^\circ, \quad \text{otherwise} \tag{9.51b}$$

Another option available to the engineer is to maximize energy output in the afternoon, when electricity demand is usually highest. In this case the azimuth angle of the module can be set somewhat to the west of due south. However, doing so would sacrifice morning electricity production and total yield for the day.

Table 9.7 Percentage of Additional Irradiation at Optimal Tilt Relative to Horizontal for Various Latitudes

Latitude (°)	Additional Global Irradiation at Optimal Tilt Relative to Horizontal
0	0%
10	1%
20	3%
30	10%
40	17%
50	26%
60	33%
65	35%
70	33%
80	22%
90	0%

The yield benefit of tilting increases as one moves away from the equator and the sun is lower in the sky. The effect of global irradiation on an optimally tilted surface relative to a horizontal surface is quantified in Table 9.7 (Chang, 2009). The increase in irradiation reaches a maximum of 35% at latitude 65° north, before declining again at higher latitudes and falling to zero at the poles.

The main cost of tilting a PV module from horizontal is the more elaborate mounting structure required, which must also be made stronger because of the higher wind loads occurring on an inclined module. Aesthetically, a raised structure on a roof is often considered to be less attractive than a flush one. Tilting may also require wider spacing between module rows to prevent self-shading, as shown in Section 9.6.3.

For these reasons the most suitable locations for fixed tilting of PV modules tend to be large flat roofs of commercial buildings and ground-mounted systems, especially at higher latitudes, whereas residential houses usually take advantage of the existing slope of their roofs.

A further consideration when deciding whether to tilt a fixed PV module is the proportion of direct and diffuse irradiation at the location. On cloudy days, nearly all global irradiation is diffused. In such conditions a module's yield is in fact maximized by laying it flat, exposing it to the full dome of the sky (Kelly and Gibson, 2009, 2011).

9.6.2 Trackers

PV modules can also be mounted on single- or double-axis trackers, with the effect on solar flux received throughout the year described in Section 2.2.1. Single-axis tracking increases annual yield in the order of 25% relative to fixed PV modules and, more importantly, it greatly increases power output in the afternoon when a demand is high. At lower latitudes such trackers are typically aligned horizontally, which is mechanically simple and allows for long tracker rows with many PV modules attached to each tracker. As latitude increases there is greater yield benefit from tilting modules to the south, and greater use is made of inclined- or vertical-axis trackers. Trade-offs of inclining the axis

include mechanical complexity and cost, higher wind loads, fewer PV modules per tracker, and greater distance between trackers to avoid shading.

Compared to single-axis trackers, double-axis ones achieve a modest additional increase in yield—typically in the range of 5–10% (Kelly and Gibson, 2009, 2011)—yet they are significantly more mechanically complex. Therefore they are mainly used in concentrating PV systems whose focusing optics must be accurately aligned with the sun in order to function (see Section 9.7).

Single-axis trackers have traditionally been used with high-efficiency crystalline silicon modules, as trackers represent a fixed cost and there is incentive to maximize energy production from each one. The use of thin-film modules on horizontal trackers is uncommon but does occur, especially when suited by local climate. In deserts, for example, thin-film modules tend to yield more electricity than crystalline modules of the same rated power because of the lower reduction in their efficiency at high temperatures (Huld et al., 2010; Kullmann, 2009).

9.6.3 Shading

When PV modules are tilted there is the risk that modules may shade each other, especially when the sun is low in the sky. It is usually not practical to completely eliminate shading, however, as when the sun is just above the horizon a very great distance between modules would be needed. Allowing some shading is mitigated by the fact that there is little solar irradiation at dawn and dusk, so the yield sacrificed is small. Similarly there is less irradiation in winter, when shading is most severe.

Although these phenomena mitigate the effect of shading, module circuitry amplifies it because cells in a PV module are connected in series. Therefore, if one cell is shaded it operates as a diode in reverse bias, decreasing the voltage of its circuit and potentially making the module's maximum power point difficult to locate (Lisell and Mosey, 2010). Therefore shading can decrease a module's output by a much greater proportion than the area shaded—more than 30 times in certain scenarios (Deline, 2009). PV cells of different materials vary in their sensitivity to this effect, while (in crystalline silicon modules) electronics can be employed that bypass shaded or failed cells. Therefore the response of specific modules to partial shading is important to consider when designing the layout of a PV system, and good design of the modules is required to avoid having a large area of PVs working at low efficiency.

The optimal amount of allowed shading is also heavily influenced by variables specific to each solar project, both economic—the relative costs of land, electricity and PV modules—and environmental, such as the proportion of direct to diffuse irradiation and surroundings topography. Sufficient space must also be left between module rows for access for repairs and maintenance.

These numerous unknowns make it impossible to provide rules of thumb for spacing of PV-module rows. Nevertheless it is instructive to examine the geometric relation between spacing and shading, particularly for the common situations of fixed tilted and E–W horizontal-tracked modules. More details on the row shading are presented in Chapter 5, Section 5.4.2. For a fixed tilted PV module facing due south Eq. (5.47a) and Eq. (5.47b) apply.

Consider a module at latitude 30°N and inclined at the same angle. The ratio of the northern shadow length to the module length (in the N–S direction) throughout the year and day is shown in Table 9.8. During the equinoxes, when all shadows on Earth move due eastward, its shadow falls 1.15 times the module height from its base. Throughout the day of the summer solstice, the shadow is shorter than the module length if it were laid flat. At the winter solstice the shadow cast is more than 1.5 times the module height throughout the day.

Table 9.8 Ratio of North-Shadow Length to Module Height for Different Days of the Year

	Ratio of North-Shadow Length to Module Length		
Time of Day	**Summer Solstice**	**Equinox**	**Winter Solstice**
6:00 am	0.00	1.15	»1
7	0.59	1.15	»1
8	0.77	1.15	2.31
9	0.88	1.15	1.79
10	0.90	1.15	1.62
11	0.92	1.15	1.56
12:00 pm	0.92	1.15	1.54
13	0.92	1.15	1.56
14	0.90	1.15	1.62
15	0.88	1.15	1.79
16	0.77	1.15	2.31
17	0.59	1.15	»1
18	0.00	1.15	»1

The above discussion applies to multiple rows of fixed, south-facing PV modules, where shadow length falling to the north dictates row spacing. We now consider rows of PV modules on single-axis trackers whose axes run north–south (a configuration seen in some large PV fields), and where shadow lengths to the west and east determine row spacing.

In this case the module tilt angle, β, varies throughout the day as the tracker follows the sun. Nominally the tilt angle would be set perpendicular to the sun's altitude, i.e., $\beta = \pi/2 - \alpha$ (or equal to the zenith angle). However when the sun is low on the horizon, the modules would be tilted almost vertical, creating severe shading between rows of any spacing. To overcome this, computer-controlled trackers can be employed that decrease the module's tilt in the early morning and late afternoon, a technique known as back-tracking. The increase in electricity yield from the avoided shading more than offsets the decrease in yield from greater incidence angle of sunlight on the modules during these times. Back-tracking allows module rows to be more closely spaced for the same yield, at the expense of a more sophisticated tracking control system.

9.6.4 Tilting versus spacing

Shading leads to a fundamental trade-off in the design of PV systems between tilting (fixed or tracking) and spacing (Denholm and Margolis, 2007). Tilting maximizes energy yield per unit area of module. However because tilting generally requires greater module spacing—both to reduce shading and to allow access for maintenance—it leads to a net decrease in energy yield per unit area of land, while also increasing mechanical complexity and capital cost of the system.

This effect is quantified in a simulation of tilting systems at Kansas City, which represents an energy density equal to the USA average value (Denholm and Margolis, 2007). The results are shown in Table 9.9, in which 3.5–5 m of spacing is assumed for the ground-mounted systems. It is seen that, in

Table 9.9 Results of a Simulation for Tilting PV Modules in Kansas City, USA

System Type	PV Array Power Density (W/m^2 of Land)	Incident Solar Radiation (kWh/m^2 of Modules/Day)	System Energy Density (kWh/m^2 of Land/Year)
Flat (rooftop)	135	4.31	150
10° tilt south (rooftop)	118	4.64	139
25° tilt south (ground based)	65	4.86	83
1-axis tracking, no tilt	48	5.70	73
2-axis tracking	20	6.60	35

Denholm and Margolis (2007).

terms of yield per land area, the greater yield per module from tilting and tracking is outweighed by the greater spacing.

It follows that a key relationship that determines the attractiveness of tilting is that between the price of PV modules and the price of land (or roof space). Expensive modules and cheap land make it attractive to tilt those modules; expensive land and cheap modules encourages maximizing yield per land area through less tilt and closer spacing. The dramatic fall in PV module prices in recent years has thus decreased the relative attractiveness of tilting and tracking.

9.7 Concentrating PV

A way to increase the effectiveness of PVs is to concentrate sunlight on small, highly efficient photovoltaic cells using inexpensive reflective material, lenses, or mirrors. These are known as *concentrating photovoltaics* (CPVs). Today, the technology takes up a very small portion of the solar industry; however, it is expected that the CPV industry will grow as technology improves and cost comes down and further field tests and demonstrations are conducted.

The solar spectrum has photons ranging up to 4 eV. A single-material PV cell can convert only about 15% of the available energy to useful electrical power. To improve this performance, multiple cells with different band gaps, which are more complex and therefore more expensive, can be used. These are called *multi-junction PVs*. Particularly, a triple-junction PV produced recently achieved a remarkable 40% efficiency (Noun, 2007). This PV consists of three layers of PV material placed one atop the other. Each of the three materials captures a separate portion of the solar spectrum (see Figure 2.26) and the objective is to capture as much of the solar spectrum as possible. These are much more expensive than other silicon solar cells, but their efficiency offsets their high cost, and in concentrating systems, a small area of these cells is required.

The advantages of CPV systems are the following:

1. They replace expensive PV material with lower-cost mirrors or reflective materials.
2. Solar cells are more efficient at high-irradiation levels.
3. Due to tracking, production of energy starts earlier in the morning and extends later in the day.

4. They have high efficiencies of around 30–40% at the module level (RENI, 2012) and 25% at the system level (i.e., including losses from inverters and tracking).
5. Due to 2-axis tracking and high efficiency modules, they produce a large amount of energy from a given surface area.

Disadvantages of CPV systems include:

1. At high concentration, cells heat up and lose efficiency, so they must be cooled.
2. Concentrating systems use only direct solar radiation, "wasting" diffuse radiation.
3. The system must track the sun; higher concentration requires more accurate tracking.
4. Concentrating systems are more complex than flat-plate ones and less reliable, because they have moving parts.
5. Two-axis trackers require relatively wide spacing to avoid shading, which reduces CPV's power output per area of land.

Compared to flat-plate PV, concentrating PV has a greater capital cost of $4–$6 per Watt and a higher conversion efficiency of direct irradiation. With this profile, CPV systems are suited to utility-scale power generation in locations with significant insolation and clear skies, such as deserts far from coasts. In such settings CPV is able to produce electricity at among the lowest cost per kWh of solar technologies.

Usually CPV uses lenses to concentrate sunlight onto small-size photovoltaic cells. Because a CPV module needs much less cell material than a traditional PV module, it is cost-effective to use higher-quality cells to increase efficiency. For CPVs, all concentrating systems presented in Chapter 3 can be used. The most popular system of CPV, however, is the Fresnel lens system. As in all concentrating systems, a tracking mechanism is required to follow the sun trajectory. Usually, a number of PVs are installed in a single box and atop each a Fresnel lens is installed. A CPV system can include a number of boxes, all put in a single tracking frame. For this type of system, two-axis tracking is required. A schematic diagram of a CPV Fresnel system is shown in Figure 9.22(a) and a photograph of an actual system is shown in Figure 9.22(b). It should be noted that, in CPVs, the distribution of solar radiation on cells has to be as uniform as possible to avoid hot spots.

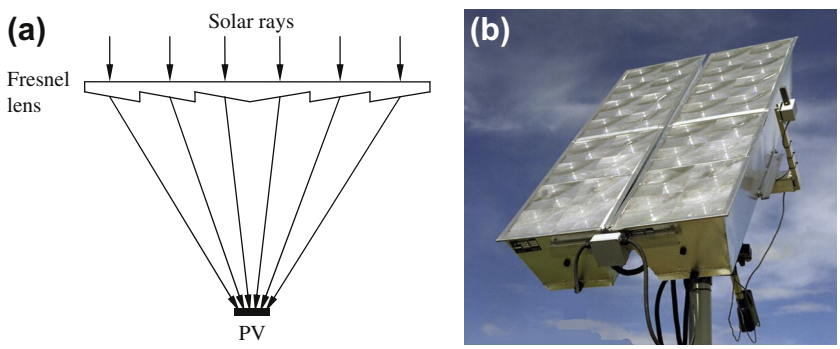

FIGURE 9.22

Schematic diagram and a photograph of a CPV Fresnel system. (a) Schematic diagram. (b) Photograph of an actual system.

Because the temperature developed in CPV systems is high, some means of removing the heat energy must be provided to avoid reduction in the PV efficiency and prolong the life of the PVs. In some systems, this extra heat is used to provide thermal energy input to other processes, as in the hybrid PV/Ts analyzed in the next section.

9.8 Hybrid PV/T systems

A system that can provide both electrical and thermal energy simultaneously would be a very interesting application. Such a system could cover part of the electrical and thermal energy needs for a number of applications in industry and buildings (hospitals, schools, hotels, and houses).

Photovoltaic panels convert solar radiation to electricity with peak efficiencies in the range of 5–20%, depending on the type of the PV cell. The efficiency of the solar cells drops with increasing operating temperatures. The temperature of PV modules increases by the absorbed solar radiation that is not converted into electricity, causing a decrease in their efficiency. For monocrystalline (c-Si) and polycrystalline (pc-Si) silicon solar cells, the efficiency decreases by about 0.45% for every degree rise in temperature. For a-Si cells, the effect is less, with a decrease of about 0.2% per degree rise in temperature, depending on the module design (see Section 9.2.2 for more details).

This undesirable effect can be partially avoided by a proper heat extraction with a fluid circulation. Natural circulation of air is the easiest way to remove heat from the PV modules and avoid the resulting efficiency drop. Hybrid PV/T collector systems may be applied, however, to achieve maximum energy output by simultaneous electricity and heat generation. In this way, the energy efficiency of the systems is increased considerably and the cost of the total energy output is expected to be lower than that of plain photovoltaic modules. The produced heat can be used to heat the building, for the production of hot water for the needs of the occupants or for low-temperature industrial applications. Stabilizing the temperature of the PV modules at a lower level is highly desirable and offers two additional advantages: an increase of the effective life of the PV modules and the stabilization of the current–voltage characteristic curve of the solar cells. Also, the solar cells act as good heat collectors and are fairly good selective absorbers (Kalogirou, 2001).

In hybrid PV/T solar systems the reduction of the PV module temperature can be combined with a useful fluid heating. Therefore, hybrid PV/T systems can simultaneously provide electrical and thermal energy, achieving a higher energy conversion rate of the absorbed solar radiation. These systems consist of PV modules coupled to heat extraction devices, in which air or water of lower temperature than that of PV modules is heated at the same time the PV module temperature is reduced. In PV/T system applications, the production of electricity is the main priority; therefore, it is necessary to operate the PV modules at low temperature to keep the PV cell electrical efficiency at a sufficient level. Natural or forced air circulation is a simple, low-cost method to remove heat from the PV modules, but it is less effective if the ambient air temperature is over 20 °C. To overcome this effect, the heat can be extracted by circulating water through a heat exchanger mounted at the rear surface of the PV module. PV/T systems provide a higher energy output than standard PV modules and could be cost-effective if the additional cost of the thermal unit is low. The water-type PV/T systems can be practical devices for water heating (mainly domestic hot water). Details of water PV/T systems are shown in Figure 9.23. For air systems, a similar design is used but, instead of the heat exchanger shown in Figure 9.23, the heat is removed by flowing air, as shown in Figure 9.24.

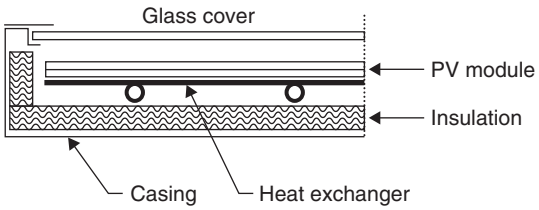

FIGURE 9.23

Details of a water PV/T collector.

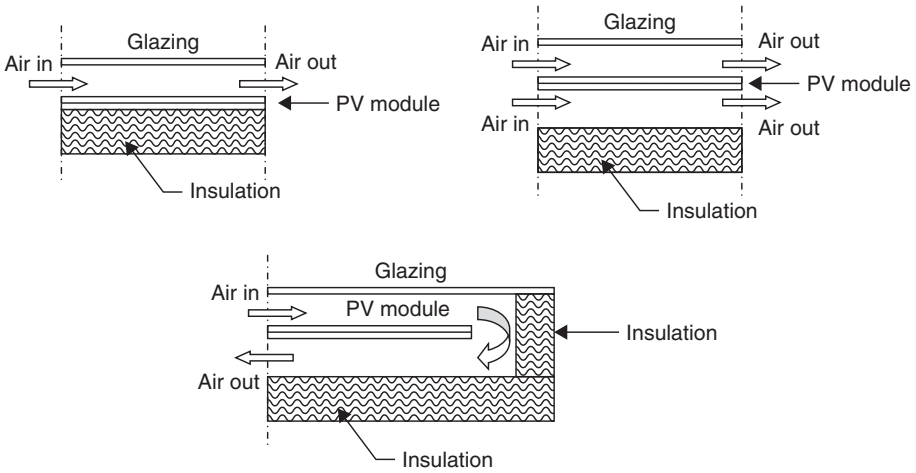

FIGURE 9.24

Details of an air PV/T collector.

Two basic types of PV/T systems can be considered, depending on the heat extraction fluid used, the water-type and the air-type PV/T systems, as shown in Figures 9.23 and 9.24, respectively. The air-type PV/T systems are of lower cost than the water-type PV/T ones and are suitable for building applications in medium- and high-latitude countries. In low-latitude countries, the ambient air temperature during the day is over 20 °C for almost half of the year, limiting the application of air-type PV/T systems to a shorter period in terms of effective electricity production. The water-type PV/T systems can be used effectively in all seasons, mainly in low-latitude countries, since water from public mains is usually under 20 °C.

Usually, the water-type PV/T models consist of silicon PV modules and the heat extraction unit is a metallic sheet with pipes for the water circulation, to avoid the direct contact of water with the PV rear surface. The heat exchanger is in thermal contact with the PV module rear surface and thermally insulated on the rear side of the heat exchanger element and the panel edges, as shown in Figure 9.23. The heat exchanger in these systems is similar to the fin and tube arrangement used in flat-plate solar collectors, so the technology of this type of system is well known to the solar industry.

In the systems shown in Figures 9.23 and 9.24, glazing is used and the final panels look like a conventional flat-plate collector. The systems, however, can also be unglazed, which is more suitable to very low-temperature applications. In the case of unglazed systems, satisfactory electrical output is obtained, depending on the operating conditions. The thermal efficiency, however, is reduced for higher operating temperatures, due to the increased thermal losses from the PV module front surface to the ambient. The addition of a glazing (like the glazing of the typical solar thermal collectors) increases significantly the thermal efficiency for a wider range of operating temperatures, but the additional optical losses from the glazing (from the additional absorption and reflection of the solar radiation) reduce the electrical output of the PV/T system.

The thermal analysis of the water and air PV/T systems are presented in the following two sections.

PV/T collectors with liquid heat recovery

The PV/T collector can be considered as a kind of solar thermal collector, which has as an absorption plate, the PV cells and a fluid heat extraction unit, in which the heat removal fluid circulates. In a water PV/T collector the heat extraction unit is usually a heat conductive plate with pipes for the circulation of the water, which is in thermal contact with PV rear side, while in air PV/T collectors it is usually an air duct placed at the rear side of the photovoltaic panel. In addition, a glazing can be used to reduce PV/T collector thermal losses, or the collector can be unglazed, to avoid the reduction in electrical output due to reflection optical losses and absorption heat losses from the glazing. The PV/T collector has also thermal insulation at the non-illuminated collector parts, similar to the way this is applied to a typical solar thermal collector. The flat-plate PV/T collector with water heat extraction can be analyzed in a similar way as a flat-plate thermal liquid collector using the basic collector model modified by Florschuetz (1979) and Tonui and Tripanagnostopoulos (2007).

Total thermal losses of PV/T collector U_L include top losses U_t, back losses U_b, and edge losses U_e, given by Eq. (3.9). These thermal losses are calculated using the same equations as the ones presented in Chapter 3, Section 3.3.2. Concerning the PV/T collector a modified heat losses coefficient $\overline{U}_L$ is used to give the reduced thermal losses due to the energy converted into electricity, given by:

$$\overline{U}_L = U_L - (\tau\alpha)\eta_{ref}\beta_{ref}G_t \tag{9.52}$$

The electrical efficiency of the PV module η_{el} depends on the temperature T_{pv} and is given by (Florschuetz, 1979):

$$\eta_{el} = \eta_{ref}\left[1 - \beta_{ref}\left(T_{pv} - T_{ref}\right)\right] \tag{9.53}$$

where

β_{ref} = temperature factor of PV efficiency (°C) and
η_{ref} = electrical efficiency for the reference temperature T_{ref}.

The thermal efficiency of the collector η_{th} is obtained by dividing the useful energy collected Q_u by the available solar energy ($A_{pv}G_t$). The useful energy is given by Eq. (3.31) or by using the collector inlet fluid temperature, T_i instead of collector plate temperature, T_p from Eq. (3.60) modified by Tonui and Tripanagnostopoulos (2007) for PV/T collectors:

$$\eta_{th} = \overline{F}_R\left[(\tau\alpha)(1 - n_{el}) - \overline{U}_L\left(\frac{T_i - T_a}{G_t}\right)\right] = \frac{\dot{m}c_p(T_o - T_i)}{A_{pv}G_t} \tag{9.54}$$

where the modified heat removal factor $\overline{F}_R$ is described by the modified collector efficiency factor $\overline{F}'$ and the two parameters differ from those of the flat-plate thermal collectors because the modified overall heat loss coefficient $\overline{U}_L$ is used instead of U_L. The relationship between $\overline{F}'$ and $\overline{F}_R$ is given by Florschuetz (1979):

$$\overline{F}_R = \frac{\dot{m}c_p}{A_{pv}\overline{U}_L}\left[1 - \exp\left(-\frac{A_{pv}\overline{U}_L\overline{F}'}{\dot{m}c_p}\right)\right] \tag{9.55}$$

PV/T Collectors with air-heat recovery

In most air solar collectors the air circulates through a channel formed between the PV solar radiation absorber and collector thermal insulation, and in some other systems through channels on both absorber (PV) sides, in one- or two-pass system (see Figure 9.24). The usual heat extraction mode is the direct air heating from the absorber rear surface by natural or forced convection. The thermal efficiency depends on channel depth, air flow mode, and air flow rate. Small channel depth and high flow rate increase heat extraction, but increase also pressure drop, which reduces the system net energy output in case of forced air flow, because of the increased power for the fan. In applications with natural air circulation, the small channel depth reduces air flow and therefore the heat extraction. In these systems a relatively large depth of air channel of about 0.1 m is necessary.

In the analysis of air PV/T collector performance the energy balance and thermal losses equations used in water PV/T collectors can be also applied. In a detailed analysis the air duct dimensions and other air circulation channel geometrical and air flow characteristics should be considered, similar to the analysis of air thermal collectors presented in Chapter 3, Section 3.4. The modified overall heat loss coefficient $\overline{U}_L$ and heat removal factor $\overline{F}_R$ for the air PV/T collectors can be also obtained from the formulas of Florschuetz (1979). For the air PV/T collector, the collector modified efficiency factor $\overline{F}'$ is calculated from Eq. (3.79) by replacing U_L by $\overline{U}_L$.

The steady-state thermal efficiency of the air PV/T collector can be calculated from Eq. (9.54).

9.8.1 Hybrid PV/T applications

The hybrid PV/T systems are considered an alternative to plain PV modules in several applications. They can be used effectively for converting the absorbed solar radiation into electricity and heat, therefore increasing their total energy output. In these systems, PV modules are coupled to heat extraction devices, in which water or air is heated and at the same time the PV module temperature is reduced to keep electrical efficiency at a sufficient level. Water-cooled PV/T systems are practical systems for water heating. These new solar energy systems are of practical interest for many applications, as they can effectively contribute to cover both the electrical and thermal loads.

It should be noted that the cost of the thermal unit remains the same irrespective of the type of PV material used, but the ratio of the additional cost of the thermal unit per PV module cost is almost double when amorphous silicon modules are used rather than the crystalline silicon ones. In addition, amorphous silicon PV modules present lower electrical efficiency, although the total energy output (electrical plus thermal) is almost equal to that of crystalline silicon PV modules.

The additional thermal output provided from the PV/T systems makes them cost-effective compared to separate PV and thermal units of the same total aperture surface area. In PV/T system applications, the production of electricity is the main priority; therefore, it is more effective to operate the PV modules at low temperature to keep a PV cell electrical efficiency at a sufficient level.

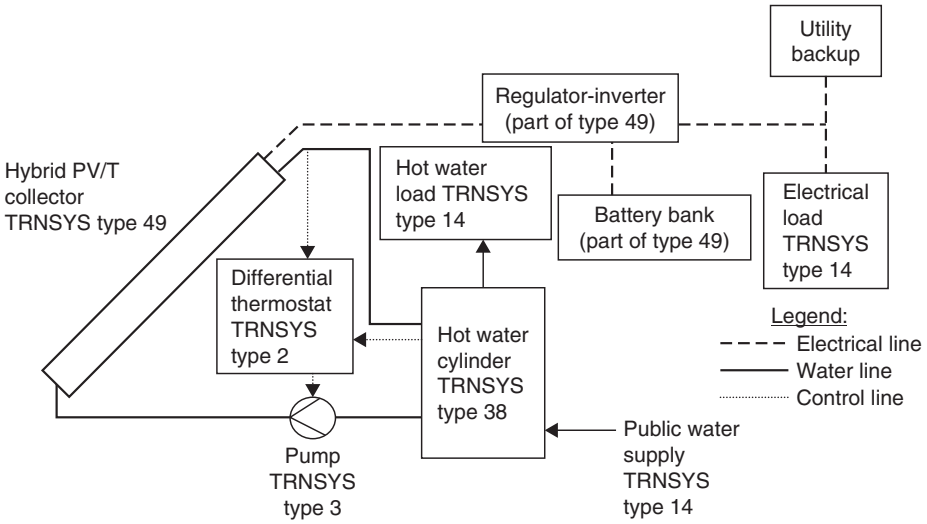

FIGURE 9.25

Hybrid PV/T system schematic.

The daily and monthly performance of a hybrid PV/T system is investigated through modeling and simulation using the TRNSYS program (see Chapter 11, Section 11.5.1). Such a system provides more electrical energy than a standard photovoltaic system because it operates at a lower temperature; in addition, thermal energy is obtained, which can be used for water heating. As shown in Figure 9.25, the system consists of a series of PV panels, a battery bank, and an inverter, whereas the thermal system consists of a hot water storage cylinder, a pump, and a differential thermostat (Kalogirou, 2001). In each case, the TRNSYS-type number used is indicated.

A copper heat exchanger is installed at the back of the photovoltaic panel, and the whole system is enclosed in a casing in which insulation is installed at the back and sides and a single low-iron glass is installed at the front to reduce the thermal losses (see Figure 9.23). Water is used as a heat transfer medium. The system also employs eight batteries connected in a 4×2 mode, i.e., four batteries in parallel and two in series.

The findings from this investigation are very promising. In addition to the increased electrical energy produced by the system, almost 50% of the hot water needs of a four-person family are satisfied with such a system, and because of the heat removal, the PV cells' annual efficiency increased considerably.

In another case the application of water PV/T systems in industry has been studied. Water-type PV/T systems were also considered for this application. The PV/T systems can be used in several industrial applications, but the most suitable are applications that need heat in low (60–80 °C) and mainly very low (<50 °C) temperatures, since in these cases, both the electrical and the thermal efficiency of the PV/T system can be kept at an acceptable level. It should be noted that the fraction of heat demand at low temperatures is high, especially in the food, brewery and beverage industries and in the paper and textile industries, where its shares could be up to 80% of the overall thermal energy needs. For example, water-cooled PV/T systems could heat water for washing or cleaning processes.

The PV/T collectors could be installed on the ground or on either flat or saw-tooth roofs, or on the façade of a factory (Kalogirou and Tripanagnostopoulos, 2007).

Finally, the performance and financial improvement of the PV/T systems was compared to the standard PV systems for building applications and proved very beneficial (Kalogirou and Tripanagnostopoulos, 2006). Additionally, it was proven that PV/T systems could be beneficial to the greater diffusion of PV units. This is especially important for countries with good penetration of solar water heaters, where it is a habit to produce hot water with solar energy. In these cases, it would be difficult to convince potential customers to install a PV system, whereas a hybrid system producing both electricity and hot water has better chances of success.

9.8.2 Water and air-heating BIPV/T

Building-integrated PV, called BIPV, is examined in a previous section. When this is combined with heat extraction it is called BIPV/T. This can be used with water or air fluid circulation. When a BIPV/T heat removal uses water (usually an aqueous propylene glycol solution) as the working fluid, the cost is much higher due to the required plumbing, more complex facade and the need to build hydronic systems integration and greater weight. Careful system output optimization of water-heating BIPV/T systems is therefore required to justify the initial capital cost investment. Although BIPV hydronic heat removal will improve PV efficiency, if the water circulation stops, for example from a pump failure, the very high consequential panel temperatures will adversely affect PV durability (Affolter et al., 2000). Furthermore the thermal efficiency of a BIPV/T collector is lower than a solar thermal flat-plate collector due to the lack of an aperture cover to inhibit convective heat loss. The solution would be to add a glazed cover which however, as seen before, will reduce the PV performance due to increase of PV optical losses and raise of PV temperature. For a large façade area structural and cost constraints may also be a problem.

Flat-plate air-heating BIPV/T collectors also yield an optimal combination of both electrical and thermal conversion efficiencies. A BIPV/T facade could act as an unglazed thermosiphon photovoltaic-thermal air-heating collector to provide natural ventilation in summer, preheated air in winter and electrical output throughout the year. A duct arranged behind the PV module allows air flow induced by buoyancy from the back of the PV panel and this air movement is governed by a combination of natural convection and wind-induced flow (Batagiannis and Gibbons, 2001). The temperature attained by the BIPV/T system depends on the incident solar energy, surface area, ambient air temperature, flow conditions, radiant surfaces, and the flow and temperature distribution (Mosfegh and Sandberg, 1998; Brinkworth et al., 1997; Tonui and Tripanagnostopoulos, 2008). It should be noted that for air flow in a PV rear-duct section, wind blowing from one direction may assist the air movement, and achieve greater cooling of the modules, whereas wind blowing from another direction may act against the required air flow direction, and reduce the cooling potential (Batagiannis and Gibbons, 2001). Additionally, for a naturally ventilated BIPV/T cladding element, buoyancy forces are balanced by the pressure drops due to the friction at the entrance and exit (Brinkworth et al., 2000). For zero wind velocity, the flow through the ventilated stack is driven only by buoyancy forces, whereas in all the other cases the flow inside the duct is due to a mixture of free and forced convection. Buoyancy induced air flow in a duct between the BIPV and the wall, even with a low mean air velocities can reduce BIPV operating temperature by about 15–20 °C giving also a 15% increase in electrical conversion efficiency (Brinkworth et al., 1997).

Exercises

9.1 Find the wavelength of radiation whose photons have energy equal to the band gap of cuprous sulfide (Cu_2S) cell (1.80 eV), compounds of cadmium sulfide (CdS) cell (2.42 eV), and gallium arsenide (GaAs) cell (1.40 eV).

9.2 A beam of blue light with wavelength of 0.46 μm and intensity of 1 mW strikes a solar cell. Estimate the number of photons incident on the cell.

9.3 The dark saturation current of a solar cell is 1.75×10^{-8} A when the cell is at 35 °C and the short-circuit current when in sunlight is 4 A. Estimate the open-circuit voltage, the maximum power output of the cell, and the number and arrangement of cells required to make a panel to supply 90 W at 12 V.

9.4 A PV system gives 9 A when the solar radiation is 750 W/m^2. How many amperes will it give at 850 W/m^2?

9.5 A 6 m^2 PV system gives 24 V and 18 A when exposed to solar radiation of 750 W/m^2. Estimate the cells' efficiency.

9.6 A PV system is required to produce 96 W at 12 V. Using solar cells that have I_{max} equal to 250 A/m^2 and V_{max} equal to 0.4 V, design the PV panel, working at the maximum power point, if each cell is 80 cm^2 in area.

9.7 Estimate the daily load and the peak power required by a PV system that has the following equipment connected:
Four lamps, 15 W each, operated from 6 pm to 11 pm.
Television, 80 W, operated from 6 pm to 11 pm.
Computer, 150 W, operated from 4 pm to 7 pm.
Radio, 25 W, operated from 11 am to 6 pm.
Water pump, 50 W, operated from 7 am to 10 am.

9.8 A remote cottage has the following loads. Estimate the daily load and peak power to be satisfied by a 24 V PV system.

Appliance	Type	Power (W)	Daytime Run (h)	Nighttime Run (h)
5 Lamps	DC	11 W each	0	5
Television	AC	75 W	2	4
Computer	AC	160 W	4	3
Radio	DC	25 W	3	1
Water pump	AC	60 W (6 A start current)	1	1
Stove	AC	1200 W	2	1

9.9 Using the loads of Exercise 9.8, estimate the expected daily energy requirement if the efficiency of the inverter is 91%, of the battery is 77%, and of the distribution circuit is 96%.

9.10 If the array and the power conditioning system losses are 10%, find the total energy delivered for a grid-connected system, assuming the efficiency of the inverter equals 90%, of the distribution circuit equals 95%, and a grid absorption rate of 90%. The energy delivered by the PV array is 500 Wh.

9.11 A south-facing PV panel is installed at 35° in a location that is at 40°N latitude. If, on May 15 noon, the beam radiation is 685 W/m^2 and the diffuse radiation is 195 W/m^2, both on a horizontal surface, estimate the absorbed solar radiation on the PV panel. The thickness of glass cover on PV is 2 mm, the extinction coefficient K is 4m^{-1}, and ground reflectance is 0.2.

9.12 If, for a PV module operating under NOCT conditions, the cell temperature is 44 °C, determine the cell temperature when this module operates at a location where $G_t = 725$ W/m^2, $V = 1$ m/s, $T_a = 35$ °C, and the module is operating at its maximum power point. The dark saturation current of a solar module is 1.7×10^{-8} A/m^2 and the short-circuit current is 250 A/m^2.

9.13 Using the simple design method, design a PV system using 60 W, 12 V panels and 145 Ah, 6 V batteries. The PV system is required to offer 3 days of storage, the battery efficiency is 75%, and the depth of discharge is 70%. The location where the system is located has 6 h of daylight during wintertime and the application is 24 V with a load of 1500 Wh.

References

Affolter, P., Ruoss, D., Tuggweiler, P., Haller, A., 2000. New generation of hybrid solar PV/T collectors. Final Report DIS56360/16868, June.

Archer, M.D., Hill, R. (Eds.), 2001. Clean Electricity from Photovoltaics, vol. 1. Imperial College Press, London, UK.

ASHRAE, 2004. Handbook of Systems and Applications. ASHRAE, Atlanta.

Barbose, G., Darghouth, N., Wiser, R., Seel, J., 2011. Tracking the Sun IV: An Historical Summary of the Installed Cost of Photovoltaics in the United States from 1998 to 2010. Lawrence Berkeley National Laboratory, p. 61.

Batagiannis, P., Gibbons, C., 2001. Thermal assessment of silicon-based composite materials used in photovoltaics. In: Conference Proceedings of Renewable Energy in Maritime Island Climates, Belfast, UK, pp. 151–157.

Blaesser, G., 1997. PV system measurements and monitoring the European experience. Sol. Energy Mater. Sol. Cells 47, 167–176.

Brinkworth, B.J., Cross, B.M., Marshall, R.H., Hongxing, Y., 1997. Thermal regulation of photovoltaic cladding. Sol. Energy 61 (3), 169–178.

Brinkworth, B.J., Marshall, R.H., Ibarahim, Z., 2000. A validated model of naturally ventilated PV cladding. Sol. Energy 69 (1), 67–81.

Chang, T.P., 2009. The Sun's apparent position and the optimal tilt angle of a solar collector in the northern hemisphere. Sol. Energy 83 (8), 1274–1284.

Coutts, T.J., 1999. A review of progress in thermophotovoltaic generation of electricity. Renewable Sustainable Energy Rev. 3 (2–3), 77–184.

De Soto, W., Klein, S.A., Beckman, W.A., 2006. Improvement and validation of a model for photovoltaic array performance. Sol. Energy 80 (1), 78–88.

Deline, P., 2009. Partially shaded operation of a grid-tied PV system. In: Proceedings of Photovoltaic Specialists Conference (PVSC) IEEE, 7–12 June 2009, Philadelphia, Pennsylvania, USA.

Denholm, P., Margolis, R., 2007. The Regional Per-Capita Solar Electric Footprint for the United States. National Renewable Energy Laboratory. Technical Report NREL/TP-670-42463.

Duffie, J.A., Beckman, W.A., 2006. Solar Engineering of Thermal Processes, third ed. Wiley & Sons, New York.

Egido, M., Lorenzo, E., 1992. The sizing of stand-alone PV systems: a review and a proposed new method. Sol. Energy Mater. Sol. Cells 26 (1–2), 51–69.

EPIA, 2010. Global Market Outlook for Photovoltaics until 2014. European Photovoltaic Industry Association. May 2010 update, p. 28.
Fanney, A.H., Dougherty, B.P., Davis, M.W., 2002. Evaluating building integrated photovoltaic performance models. In: Proceedings of the 29th IEEE Photovoltaic Specialists Conference (PVSC), New Orleans, LA.
Florschuetz, L.W., 1979. Extension of the Hottel -Whillier model to the analysis of combined photovoltaic/thermal flat plate collectors. Sol. Energy 22 (2), 361–366.
Fragaki, A., Markvart, T., 2008. Stand-alone PV system design: results using a new sizing approach. Renewable Energy 33 (1), 162–167.
Fthenakis, V.M., Kim, H.C., 2011. Photovoltaics: life-cycle analyses. Sol. Energy 85 (8), 1609–1628.
Hansen, A.D., Sorensen, P., Hansen, L.H., Binder, H., 2000. Models for a Stand-Alone PV System. Riso National Laboratory, Roskilde, Denmark. Riso-R-1219(EN)/SEC-R-12.
Hashimoto, O., Shimizu, T., Kimura, G., 2000. A novel high performance utility interactive photovoltaic inverter system. In: 35th IAS Annual Meeting and World Conference on Industrial Applications of Electrical Energy, October, Rome, Italy, pp. 2255–2260.
Hontoria, L., Aguilera, J., Zufiria, P., 2005. A new approach for sizing stand-alone photovoltaic systems based in neural networks. Sol. Energy 78 (2), 313–319.
Huld, T., Gottschalg, R., Beyer, H.G., Topic, M., 2010. Mapping the performance of PV modules, effects of module type and data averaging. Sol. Energy 84 (2), 324–328.
Jardine, C.N., Lane, K., Conibeer, G.J., 2001. PV-Compare: direct comparison of eleven PV technologies at two locations in Northern and Southern Europe. In: Proceedings of the 17th European Conference on Photovoltaic Solar Energy Conversion, Munich, 2001.
Kalogirou, S.A., 2001. Use of TRNSYS for modelling and simulation of a hybrid PV-thermal solar system for Cyprus. Renewable Energy 23 (2), 247–260.
Kalogirou, S.A., Tripanagnostopoulos, Y., 2006. Hybrid PV/T solar systems for domestic hot water and electricity production. Energy Convers. Manage. 47 (18–19), 3368–3382.
Kalogirou, S.A., Tripanagnostopoulos, Y., 2007. Industrial application of PV/T solar energy systems. Appl. Therm. Eng. 27 (8–9), 1259–1270.
Kazmerski, L., 1997. Photovoltaics: a review of cell and module technologies. Renewable Sustainable Energy Rev. 1 (1–2), 71–170.
Kelly, N., Gibson, T., 2009. Improved photovoltaic energy output for cloudy conditions. Sol. Energy 83 (11), 2092–2102.
Kelly, N., Gibson, T., 2011. Increasing the solar photovoltaic energy capture on sunny and cloudy days. Sol. Energy 85 (1), 111–125.
King, D.L., Kratochvil, J.E., Boyson, W.E., Bower, W.I., 1998. Field experience with a new performance characterization procedure for photovoltaic arrays. In: Proceedings of the Second World Conference and Exhibition on Photovoltaic Solar Energy Conversion on CD ROM, Vienna, Austria.
King, D.L., Boyson, W.E., Kratochvil, J.E., 2004. Photovoltaic Array Performance Model. Sandia National Laboratories. Report SAND 2004–3535.
Kjar, S.B., Pederson, J.K., Blaabjerg, F., 2005. A review of simple-phase grid-connected inventors for photovoltaic modules. IEE Trans. Ind. Appl. 41, 1292–1306.
Kullmann, S., 2009. Specific Energy Yield of Low-Power Amorphous Silicon and Crystalline Silicon Photovoltaic Modules in a Simulated Off-Grid, Battery-Based System. MSc Thesis. Humboldt State University, p. 123.
Lasnier, F., Ang, T.G., 1990. Photovoltaic Engineering Handbook. Adam Higler, Princeton, NJ, p. 258.
Lisell, L., Mosey, G., 2010. Feasibility Study of Economics and Performance of Solar Photovoltaics at the Former St. Marks Refinery in St. Marks, Florida. National Renewable Energy Laboratory. Technical Report, NREL/TP-6A2–48853.

Lorenzo, E., 1994. Solar Electricity Engineering of Photovoltaic Systems. Artes Graficas Gala, S.L., Madrid, Spain.
Marion, B., 2008. Comparison of Predictive Models for PV Module Performance. National Renewable Energy Laboratory. May 2008, NREL/CP-520–42511, p. 9.
Markvart, T., Fragaki, A., Ross, J.N., 2006. PV system sizing using observed time series of solar radiation. Sol. Energy 80 (1), 46–50.
Mellit, A., Benghanem, M., Hadj Arab, A., Guessoum, A., 2005. An adaptive artificial neural network for sizing of stand-alone PV system: application for isolated sites in Algeria. Renewable Energy 3 (10), 1501–1524.
Mosfegh, B., Sandberg, M., 1998. Flow and heat transfer in air gap behind photovoltaic panels. Renewable Sustainable Energy Rev. 2, 287–301.
Nelson, J., 2002. Organic photovoltaic films. Curr. Opin. Solid State Mater. Sci. 6 (1), 87–95.
Norton, B., Eames, P.C., Mallick, T.K., Huang, M.J., McCormack, S.J., Mondol, J.D., Yohanis, Y.G., 2011. Enhancing the performance of building integrated photovoltaics. Sol. Energy 85 (8), 1629–1664.
Noun, B., 2007. Solar power. Renewable Energy, 2007/2008, WREN, 62–63.
Photon, January 2012. 27.7 GW of Grid-Connected PV Added in 2011. Photon.
Photon, August 2012. Global Installed PV Capacity in 2012. Photon.
Price, S., Margolis, R., (Primary Authors), January 2010. 2008 Solar Technologies Market Report. National Renewable Energy Laboratory, p. 131.
RENI, April 2012. PV Power Plants 2012 – Industry Guide. RENI Renewables Insight, p. 108.
RENI, April 2010. PV Power Plants 2010 – Industry Guide. RENI Renewables Insight, p. 45.
Runyon, J., 2012. Staying Alive: Could Thin-Film Manufacturers Come Out Ahead in the PV Wars? Part 2. Available from: www.RenewableEnergyWorld.com.
Sayigh, A.A.M., 2008. Renewable energy 2007/2008. World Renewable Energy Network, 9–15.
Schreiber, D., 2009. PV Market Overview: Where Does the Thin Film Market Stand and Could Go? EuPD Research, Munich, p. 23.
Sick, F., Erge, T., 1996. Photovoltaics in Buildings: A Design Handbook for Architects and Engineers. James & James Limited, London, UK.
Simmons, A.D., Infield, D.G., 1996. Grid-connected amorphous silicon photovoltaic array. Prog. Photovoltaics: Res. Appl. 4, 381–388.
Tidball, R., Bluestein, J., Rodriguez, N., Knoke, S., November 2010. Cost and Performance Assumptions for Modeling Electricity Generation Technologies. National Renewable Energy Laboratory. NREL/SR-6A20-48595, p. 211.
Tonui, J.K., Tripanagnostopoulos, Y., 2007. Performance improvement of PV/T solar collectors with natural air flow operation. Sol. Energy 81 (4), 498–511.
Tonui, J.K., Tripanagnostopoulos, Y., 2008. Performance improvement of PV/T solar collectors with natural air flow operation. Sol. Energy 82 (1), 1–12.
Toyokawa, S., Uehara, S., 1997. Overall evaluation for R&D of PV modules integrated with construction materials. In: Conference Record of the IEEE Photovoltaic Specialists Conference, October, Anaheim, CA, USA, pp. 1333–1336.
Woyte, A., van den Keybus, J., Belmans, R., Nijs, J., 2000. Grid connected photovoltaics in the urban environment – an experimental approach to system optimisation. In: IEEE Proceedings for Power Electronics and Variable Speed Drives, September, pp. 548–553.